Ore Geology Reviews 90 (2017) 110–130

Contents lists available at ScienceDirect

Ore Geology Reviews

journal homepage: www.elsevier.com/locate/oregeo

Chromitites from the Luanga Complex, Carajás, Brazil: Stratigraphic distribution and clues to processes leading to post-magmatic alteration

Eduardo Teixeira Mansur, Cesar Fonseca Ferreira Filho *

Instituto de Geociências, Universidade de Brasília, Brasília-DF 70910-900, Brazil

ARTICLE INFO

Article history:
Received 7 July 2016
Accepted 14 March 2017
Available online 20 March 2017

Keywords:
Chromitite
Chromite
Silicate inclusion
Layered intrusion
Carajás

ABSTRACT

The Neoarchean (ca. 2.75 Ga) Luanga Complex, located in the Carajás Mineral Province in Brazil, is a medium-size layered intrusion consisting, from base to top, of ultramafic cumulates (Ultramafic Zone), interlayered ultramafic and mafic cumulates (Transition Zone) and mafic cumulates (Mafic Zone). Chromitite layers in the Luanga Complex occur in the upper portion of interlayered harzburgite and orthopyroxenite of the Transition Zone and associated with the lowermost norites of the Mafic Zone. The stratigraphic interval that hosts chromitites (~150 meters thick) consists of several cyclic units interpreted as the result of successive influxes of primitive parental magma. The compositions of chromite in chromitites from the Transition Zone (Lower Group Chromitites) have distinctively higher Cr# (100Cr/(Cr + Al + Fe^{3+})) compared with chromite in chromitites from the Mafic Zone (Upper Group Chromitites). Chromitites hosted by noritic rocks are preceded by a thin layer of harzburgite located 15–20 cm below each chromitite layer. Lower Cr# in chromitites hosted by noritic rocks are interpreted as the result of increased Al_2O_3 activity caused by new magma influxes. Electron microprobe analyses on line transverses through 35 chromite crystals indicate that they are rimmed and/or extensively zoned. The composition of chromite in chromitites changes abruptly in the outer rim, becoming enriched in Fe^{3+} and Fe^{2+} at the expense of Mg, Cr, Al, thus moving toward the magnetite apex on the spinel prism. This outer rim, characterized by higher reflectance, is probably related to the metamorphic replacement of the primary mineralogy of the Luanga Complex. Zoned chromite crystals indicate an extensive exchange between divalent (Mg, Fe^{2+}) cations and minor to none exchange between trivalent cations (Cr^{3+}, Al^{3+} and Fe^{3+}). This Mg-Fe zoning is interpreted as the result of subsolidus exchange of Fe^{2+} and Mg between chromite and coexisting silicates during slow cooling of the intrusion. A remarkable feature of chromitites from Luanga Complex is the occurrence of abundant silicate inclusions within chromite crystals. These inclusions show an adjacent inner rim with higher Cr# and lower Mg# (100 Mg/(Mg + Fe^{2+})) and Al# (100Al/(Cr + Al + Fe^{3+})). This compositional shift is possibly due to crystallization from a progressively more fractionated liquid trapped in the chromite crystal. Significant modification of primary cumulus composition of chromite, as indicated in our study for the Luanga Complex, is likely to be common in non-massive chromitites and the rule for disseminated chromites in mafic intrusions.

1. Introduction

Cr-bearing spinels have been used as important petrogenetic indicators in many studies (e.g., Irvine, 1965; Stowe, 1994; Barnes and Roeder, 2001). The composition of chromite, a mineral relatively resistant to alteration that crystallizes over a wide range of mafic and ultramafic magmas, is particularly useful as an indicator of magmatic processes in rocks submitted to metamorphism or hydrothermal alteration. However, chromite is susceptible to significant post-magmatic modification, as indicated by several studies of chromite in komatiites (e.g., Barnes, 2000), in ophiolitic complexes (e.g., Evans and Frost, 1975; Gole and Hill, 1990) and in chomitites from Archean greenstone belts (e.g., Mondal et al., 2006; Mukherjee et al., 2010, 2015). Primary chromite compositions inherited from the magma may also be modified due to reaction with intercumulus liquid or subsolidus reaction with silicates (e.g., Barnes, 1998; Barnes and Roeder, 2001). Mass balance arguments are commonly used to indicate that massive chromitites with >70 vol% chromite are likely to preserve its original igneous compositions because there are few other phases available for element exchange (e.g., Eales and Reynolds, 1986). This reasoning was successfully used in several studies of

* Corresponding author.
E-mail addresses: etmansur@gmail.com (E.T. Mansur), cesarf@unb.br (C.F. Ferreira Filho).

http://dx.doi.org/10.1016/j.oregeorev.2017.03.016
0169-1368/

chromitites (e.g., Bacuri Complex, Spier and Ferreira Filho, 2001; Ipueira-Medrado Sill, Marques and Ferreira Filho, 2003; Nuasahi and Sukinda Massifs, Mondal et al., 2006; Nuggihalli greenstone belt, Mukherjee et al., 2010). However, apart from massive chromitites, post-magmatic modifications should be carefully evaluated before using chromite compositions to indicate magma types, tectonic environments and magmatic fractionation.

This study, the first systematic description of chromitites throughout the stratigraphy of the Luanga Complex, provides an additional example of chromitites hosted by mafic cumulates. The stratigraphic distribution of chromitites and mineral composition data of chromite support previous results from host cumulate rocks suggesting that the Luanga layered intrusion originated in a dynamic open-system magma chamber (Mansur and Ferreira Filho, 2016). In addition, our results indicate extensive modification of primary cumulus composition of chromite in chromitites of the Luanga Complex. We discuss this composition modification considering both late-magmatic and metamorphic processes. Our results indicate that the common use of chromite composition as a petrogenetic indicator for mafic intrusions should be considered with caution.

2. Regional setting

2.1. The Carajás Mineral Province

The Carajás Mineral Province, located in the southeastern portion of the Amazonian Craton (Fig. 1A), is one of the most important mineral provinces of the South American continent, hosting several world-class Cu-Au and Ni deposits along with the largest iron resources of the world. The Carajás Mineral Province is subdivided in two Archean tectonic domains: the Rio Maria Domain to the south and the Carajás Domain to the north (Fig. 1B; Vasquez et al., 2008). A poorly defined zone characterized by regional EW faults, designated as the Transition Subdomain (Feio et al., 2013), separates these two domains.

The Rio Maria Domain is a typical granite–greenstone terrain (Vasquez et al., 2008). The Andorinhas Supergroup (Docegeo, 1988) comprises several individual Mesoarchean (ca. 2.94 Ga) greenstone belts (Macambira and Lancelot, 1996; Souza et al., 2001). The recent characterization of spinifex-textured komatiites in a greenstone belt sequence within the Transition Subdomain (Siepierski and Ferreira Filho, 2016), suggests that the Andorinhas Supergroup extends further north than indicated in previous regional maps.

The Archean basement of the Carajás Domain consists mainly of gneiss-migmatite-granulite terrains, generally related to the Xingu Complex (Docegeo, 1988; Machado et al., 1991; Pidgeon et al., 2000). Different models have been proposed to explain the evolution of the Neoarchean volcano-sedimentary sequences, which include the large sequence of metabasalts of the Grão Pará Group (ca. 2.75 Ga; Machado et al., 1991; Vasquez et al., 2008) and associated banded iron formations. An intra-plate rift model is presented in several studies (e.g., Gibbs et al., 1986; Villas and Santos, 2001) but subduction-related environments have also been proposed (e.g., Dardenne et al., 1988; Teixeira and Eggler, 1994). These volcano-sedimentary sequences are covered by low-grade metamorphic sequences of clastic sedimentary rocks from the Águas Claras Formation (Araújo et al., 1988).

Several mafic-ultramafic complexes intrude rocks of the Xingu Complex and the volcanic-sedimentary sequences in the Carajás Domain (Docegeo, 1988; Ferreira Filho et al., 2007). These intrusions host large Ni laterite deposits (e.g., Onça-Puma, Vermelho, Jacaré) as well as PGE deposits (e.g., Luanga, Lago Grande). Distinct magmatic structures and petrological evolution of the layered intrusions suggest that they include different Neoarchean magmatic suites (e.g., Rosa, 2014; Siepierski, 2016; Teixeira et al., 2015).

2.2. The Serra Leste Magmatic Suite

The Serra Leste Magmatic Suite (Ferreira Filho et al., 2007) consists of a cluster of small- to medium-size layered mafic-ultramafic intrusions located in the northeastern portion of the Carajás Mineral Province (Fig. 1). Mafic-ultramafic complexes are intrusive into gneiss and migmatites of the Xingu Complex and/or into volcano-sedimentary rocks of the Grão Pará Group. Systematic geological and petrological studies of the Lago Grande (Teixeira et al., 2015) and Luanga (Mansur and Ferreira Filho, 2016) Complexes provided the geological-petrological framework of the Serra Leste Magmatic Suite. The architecture of the intrusion and the crystallization sequence described in the Luanga and Lago Grande complexes, characterized by ultramafic cumulates overlying mafic cumulates, suggest an overturned layered sequence. Although the tectonic processes leading to the overturned sequence of layered rocks in the Lago Grande and Luanga Complexes have so far not been studied in detail, regional structural studies indicate significant tectonic transport leading to major overturned blocks (Holdsworth and Pinheiro, 2000). In both complexes, primary igneous minerals are partially replaced by metamorphic assemblages that indicate temperatures up to the lower amphibolite facies of metamorphism. This metamorphic replacement is heterogeneous (i.e., variable from minor to extensive in different portions of the intrusion) and characterized by an extensive hydration of primary minerals that largely preserves magmatic textures and bulk chemical composition.

The Luanga Complex is a 6 km long and up to 3.5 km wide layered intrusion (Fig. 2) consisting, from base to top, of ultramafic cumulates (Ultramafic Zone), an intercalation of ultramafic and mafic cumulates (Transition Zone), and mafic cumulates (Mafic Zone). The Ultramafic Zone comprises an up to 800 m thick sequence of serpentinite (i.e., metamorphosed peridotite) with thin (<10 m thick) interlayered orthopyroxenite lenses. The Transition Zone consists of an up to 800 m thick pile of interlayered ultramafic and mafic cumulate rocks. Interlayering of variably textured orthopyroxenite, harzburgite and norite (Fig. 2C) in different scales (from few centimeters up to hundreds of meters thick) is a remarkable feature of the Transition Zone. Interlayering and reversals in cryptic variation of orthopyroxene and olivine in the Transition Zone (Mansur and Ferreira Filho, 2016) support an open and dynamic magmatic system. The Mafic Zone consists of up to 2000 m thick sequence of monotonous norite and minor interlayered orthopyroxenite (Fig. 2C). Chromitite layers of variable thickness (from few centimeters up to 0.6 m thick) and textures (Fig. 3) occur mainly in the upper portions of the Transition Zone and the lowermost portion of the Mafic Zone. PGE mineralizations occur associated with base metal sulfides in the contact zone of the Ultramafic and Transition Zones and associated with chromitite layers in the Transition Zone (Diella et al., 1995; Ferreira Filho et al., 2007).

3. Sampling and analytical procedures

For this study, a drill hole representative of the Transition Zone in the central portion of the Luanga Complex was systematically sampled for unweathered rocks with primary magmatic textures and minerals (drill hole LUFD-079; Fig. 2A and B). A total of 24 samples were collected for petrographic and mineral analyses, including 6 samples of thin chromitite layers, 6 samples from the

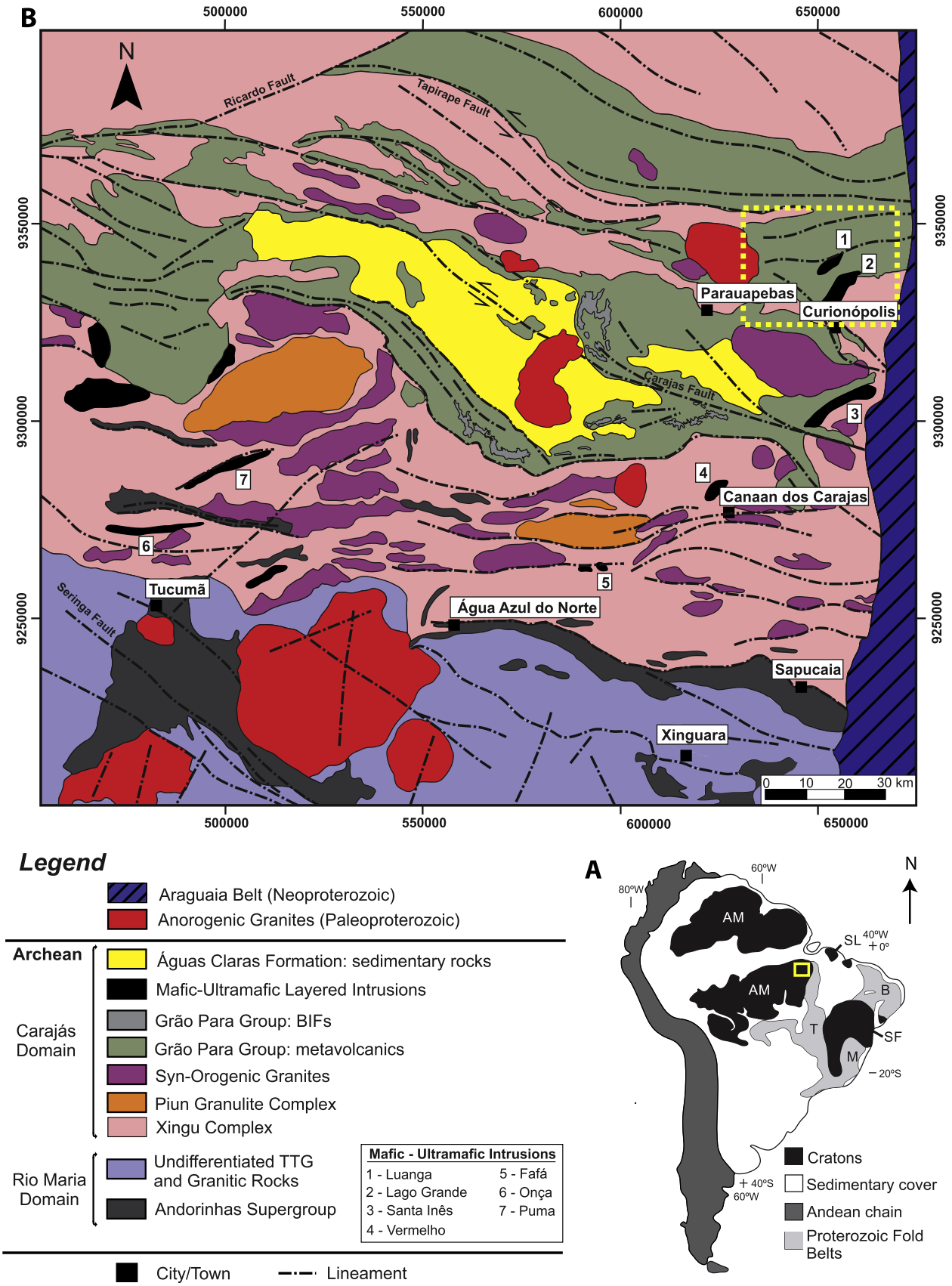

Fig. 1. (A) Location of the Carajás Mineral Province. AM- Amazonic Craton; B – Borborema Province; M – Mantiqueira Province; SF – São Francisco Craton; T – Tocantins Province. (B) Geological map of the Carajás Mineral Province (modified from Vasquez et al., 2008). The dashed rectangle indicates the location of the Serra Leste magmatic suite.

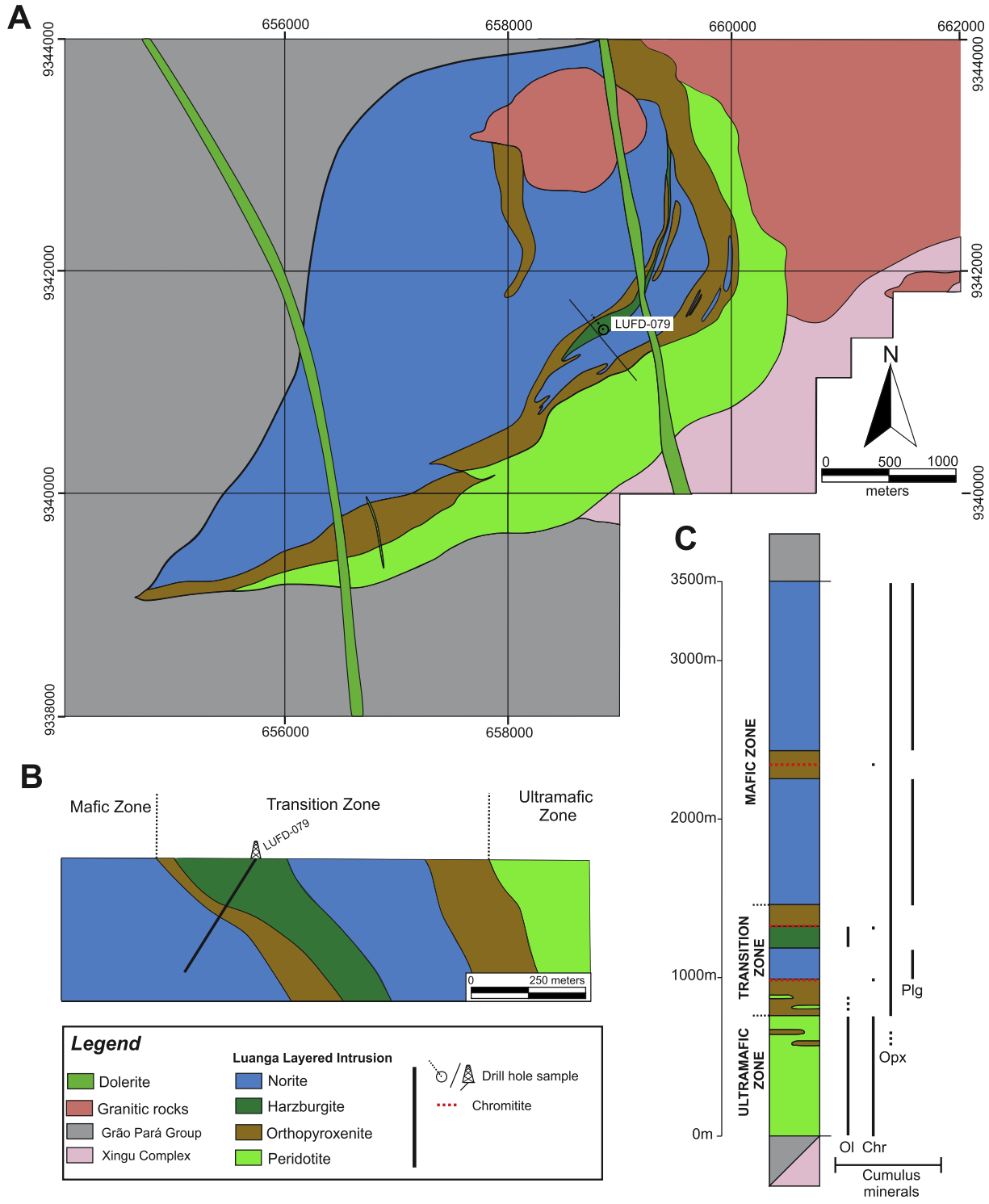

Fig. 2. (A) Geological map of the Luanga Complex (partially modified from unpublished report of VALE). Note the location of drill hole LUFD-079 referred to in this study. (B) Geological section on the central portion of the complex (partially modified from Mansur and Ferreira Filho, 2016). (C) Representative stratigraphic column for the Luanga Complex (partially modified from Mansur and Ferreira Filho, 2016). Note the variation of cumulus minerals through the stratigraphy

thickest (~60 cm) chromitite layer, and 12 samples from host cumulate rocks (Fig. 3).

Secondary electron images were taken with a JEOL JCM-5000 Neoscope, at the Micropaleontology Laboratory of the University of Brasília (Brazil), using carbon coating to enhance the contrast and definition.

Mineral analyses were performed on polished thin section using a 5 wavelength dispersive (WDS) spectrometer JEOL JXA-8230 SuperProbe at the Electron Microprobe Laboratory of the University of Brasília (Brazil). Systematic WDS analyses were obtained for chromite, orthopyroxene and plagioclase. Operating conditions for the WDS analyses were 15 kV accelerating voltage, with a beam current of 10 nA and probe diameters of 3 μm for chromite and orthopyroxene and 5 μm for plagioclase. Count times on peak and on background were 10 s and 5 s, respectively. Using these analytical conditions, detection limits are around 80 ppm. Both

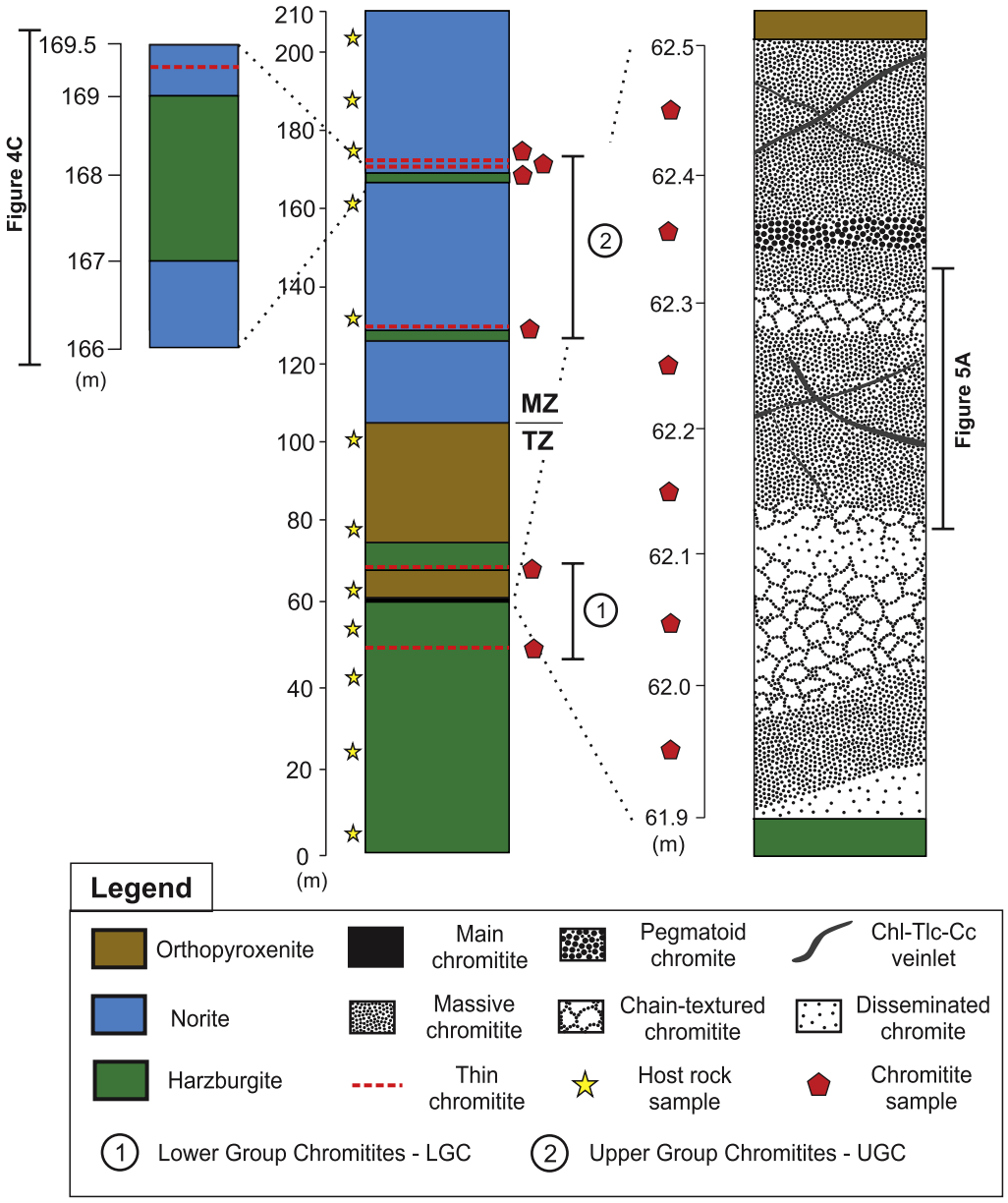

Fig. 3. Stratigraphic section of the drill core LUFD-079 (i.e., 210 meters deep; left) and a detailed section of the main chromitite (right). Note that the Luanga Complex comprises an overturned intrusion, but the stratigraphy of the drill core is shown in the original position. The location of the samples is indicated. MZ = Mafic Zone; TZ = Transition Zone.

synthetic and natural mineral standards were used for the analyses and the same standards and procedure were retained throughout the analytical work. For chromite analysis, the cation compositions were calculated following the method described by Haggerty (1976) and Robin et al. (1992), Fe^{3+} was calculated assuming perfect stoichiometry. Chromite data are presented in terms of Cr# (100Cr/(Cr + Al + F^{e3+})), Fe^{3+}# (100Fe^{3+}/(Fe^{3+}+Cr + Al)), Al# (100Al/(Al + Cr + Fe^{3+})), Mg# (100 Mg/(Mg + Fe^{2+})) and Fe^{2+}# (100Fe^{2+}/(Fe^{2+}+Mg)) throughout the paper. The complete dataset for chromite analyses is given on the Online Supplementary Table A1.

4. Geology and stratigraphy through the drill hole LUFD-079

The drill hole LUFD-079, located at the central portion of the Transition Zone (Fig. 2A and B), intersects several chromitite layers hosted by different rock types (Fig. 3). From the stratigraphic base to top the drill core comprises interlayered harzburgite and orthopyroxenite from the upper portion of the Transition Zone, and a monotonous sequence of norite with minor thin layers of harzburgite from the base of the Mafic Zone (Fig. 3). The chromite-rich layers (Fig. 3) are divided into those located in the Transition Zone (Lower Group Chromitites - LGC), and those located in the lowermost portion of the Mafic Zone (Upper Group Chromitites - UGC).

Harzburgite is a medium- to coarse-grained olivine + chromite cumulate with intercumulus orthopyroxene. Coarse-grained harzburgite usually consists of large orthopyroxene oikocrysts enclosing several olivine crystals (Fig. 4A). The modal composition is variable due to different amount of interstitial minerals, including plagioclase as an additional common intercumulus mineral. Orthopyroxenite is a medium- to coarse-grained rock with tabular orthopyroxene as cumulus mineral. The texture varies from meso to orthocumulate with plagioclase as the predominant intercumulus mineral (Fig. 4B). The thickest chromitite layer (designated main chromitite) is ~ 60 cm thick and occurs at the contact between harzburgite and orthopyroxenite (Fig. 3). Norite is a medium-

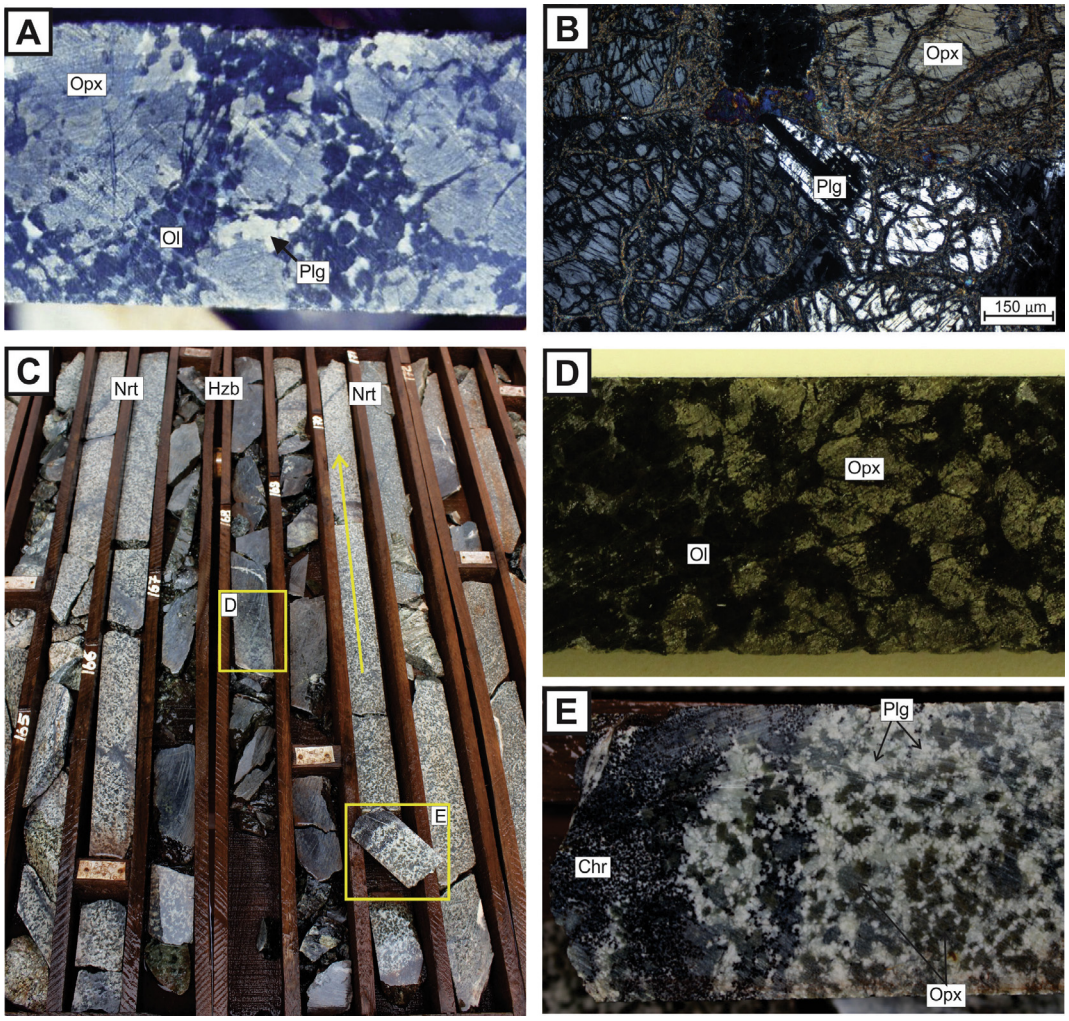

Fig. 4. Textures in chromitites and host rocks from drill core LUFD-079 (A) Coarse-grained harzburgite (Hzb) consisting of large orthopyroxene (Opx) oikocrysts enclosing several olivine (Ol – black color) crystals and minor interstitial plagioclase (Plg – white color). (B) Photomicrograph (crossed polarizers) of orthopyroxenite consisting of cumulus orthopyroxene and minor intercumulus plagioclase. (C) Harzburgite layer preceding the appearance of thin chromitite layer hosted by noritic rocks (Nrt) of the Mafic Zone. The arrow points to the bottom of the drill core, indicating that the harzburgite is located stratigraphically below the chromitite (see stratigraphic section in Fig. 3 for the location of the core). The yellow rectangles indicate the areas of photos D and E. (D) Detail of harzburgite consisting of cumulus olivine and orthopyroxene. (E) Thin chromitite (Chr) layers hosted by noritic rocks of the Mafic Zone. Note cumulus chromite grains and intercumulus plagioclase (white) and orthopyroxene (light brown). For all the photos the core is 4.7 cm wide.

grained orthopyroxene and plagioclase adcumulate rock. A thin (i.e., 2–3 m thick) harzburgite layer always occur 15–20 cm below thin chromitite layers hosted by norite (Figs. 3C, 4D and E).

Primary igneous minerals of these cumulate rocks are commonly partially replaced by metamorphic assemblages. This replacement is heterogeneous and is characterized by extensive hydration that preserves primary textures and the compositional domains of igneous minerals. These assemblages include serpentine + talc + magnetite ± cummingtonite in replaced harzburgite, talc + serpentine + magnetite ± cummingtonite in replaced orthopyroxenite (Fig. 4B), and hornblende + chlorite + epidote in replaced norite. Metamorphic assemblages indicate temperatures up to the lower amphibolite facies of metamorphism, thus consistent with those described in previous studies of the Luanga (Ferreira Filho et al., 2007) and Lago Grande Complexes (Teixeira et al., 2015).

5. The chromitite layers

5.1. Petrography

Chromitite layers intersected by drill core LUFD-079 include the main chromitite and 6 thin layers (<10 cm thick) (Fig. 3). It has sharp contacts with both the underlying harzburgite and the overlying orthopyroxenite, suggesting abrupt changes in the sequence of cumulate minerals in both contacts. The main chromitite extends for 1–2 hundred meters along strike, as indicated by drill core information, but the continuity beyond that is not constrained due to poor outcropping. Massive chromitite prevails (~ 65 vol.%) and is associated with irregular domains of chain-textured and disseminated chromitite (Figs. 3 and 5A). Massive chromitite is a fine- to medium-grained chromite cumulate with chromite grains representing more than 50 vol% (Fig. 5A). Orthopyroxene and plagioclase, commonly replaced by fine-grained aggregates of serpentine, amphibole, chlorite and talc, are typically the main interstitial minerals. Chromite occurs as euhedral to subhedral annealed crystals with discrete alteration along crystal borders and fractures (Fig. 5B). Rounded silicate inclusions inside chromite grains are common and have variable sizes (Fig. 5). The mineralogy of these inclusions consists of amphibole, chlorite and minor talc, typically the same fine-grained replacement minerals described for the matrix. Chain-textured chromitite, consisting of 15–20 vol % chromite, is characterized by orthopyroxene pseudomorphs surrounded by dozens of medium- to fine-grained chromite crystals (Figs. 5C). Fine-grained chromite grains are also enclosed by

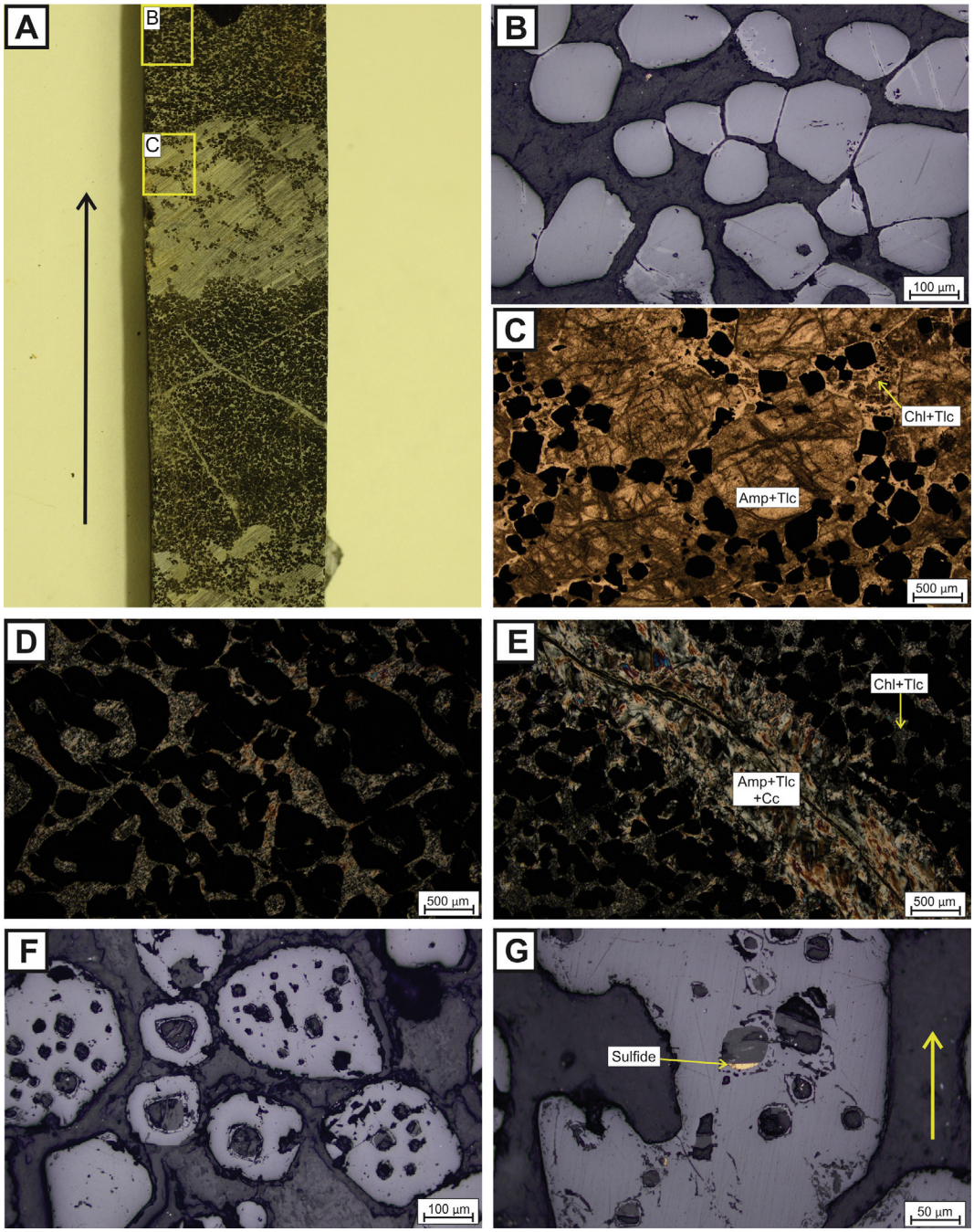

Fig. 5. Textures in chromitites. (A) Textures varying from massive, chain-textured and disseminated in the main chromitite (see Fig. 3 for location of the drill core). Primary silicates (light gray color) are replaced by a fine-grained aggregate of serpentine and talc. Carbonate-rich veinlets cross cut the chromitite. The arrow points upward the stratigraphy. (B) Photomicrograph (reflected light) of massive chromitite with polygonal contact between chromite grains. Note that chromite grains are partially altered along borders and fractures (light gray color). (C) Photomicrograph of chain-textured chromitite. Chromite crystals are interstitial to orthopyroxene pseudomorphs replaced by amphibole (Amp) and talc (Tlc). Note interstitial fine-grained aggregates of chlorite (Chl) and talc, probably resulting from alteration of intercumulus plagioclase in contact with Opx. (D) Photomicrograph (crossed polarizers) of pegmatoid chromitite. Note silicate inclusions with irregular shape in chromite grains. The intercumulus and inclusion-hosted minerals are replaced by a fine-grained aggregate of chlorite and talc. (E) Photomicrograph (crossed polarizers) of carbonate (Cc)-amphibole-talc veinlet cross cutting massive chromitite. Note that chromite grains are surrounded by a fine-grained aggregated of chlorite and talc, probably resulting from alteration of intercumulus silicates. (F) Photomicrograph (reflected light) of inclusion-bearing chromite crystals from a thin chromitite of the Mafic Zone. Note the characteristic sector zoning of inner rims adjacent to silicate inclusions. (G) Photomicrograph (reflected light) of inclusion-bearing chromite crystal highlighting the presence of a sulfide droplet at the bottom of the inclusion. The thin section is oriented and the sulfide droplet faces the base of the chromite-rich layer (the arrow points upward the stratigraphy).

orthopyroxene pseudomorphs in chain-textured chromitites (Fig. 5C). The transition from massive to chain-textured chromitite is gradational and marked by the progressive decrease in chromite modal composition. The same type of silicate inclusions observed in massive chromitites occurs in chain-textured chromitites, but they are less abundant in the latter. The disseminated chromitite contains 5–10 vol% of cumulus chromite and 95–90 vol% of variably replaced orthopyroxene and plagioclase. Chromite grains in disseminated chromitite are extensively altered and rarely have silicate inclusions. Coarse-grained chromitite is restricted to a 2 cm thick layer (see pegmatoid chromitite in Fig. 3) characterized by coarse chromite grains containing a large volume of silicate

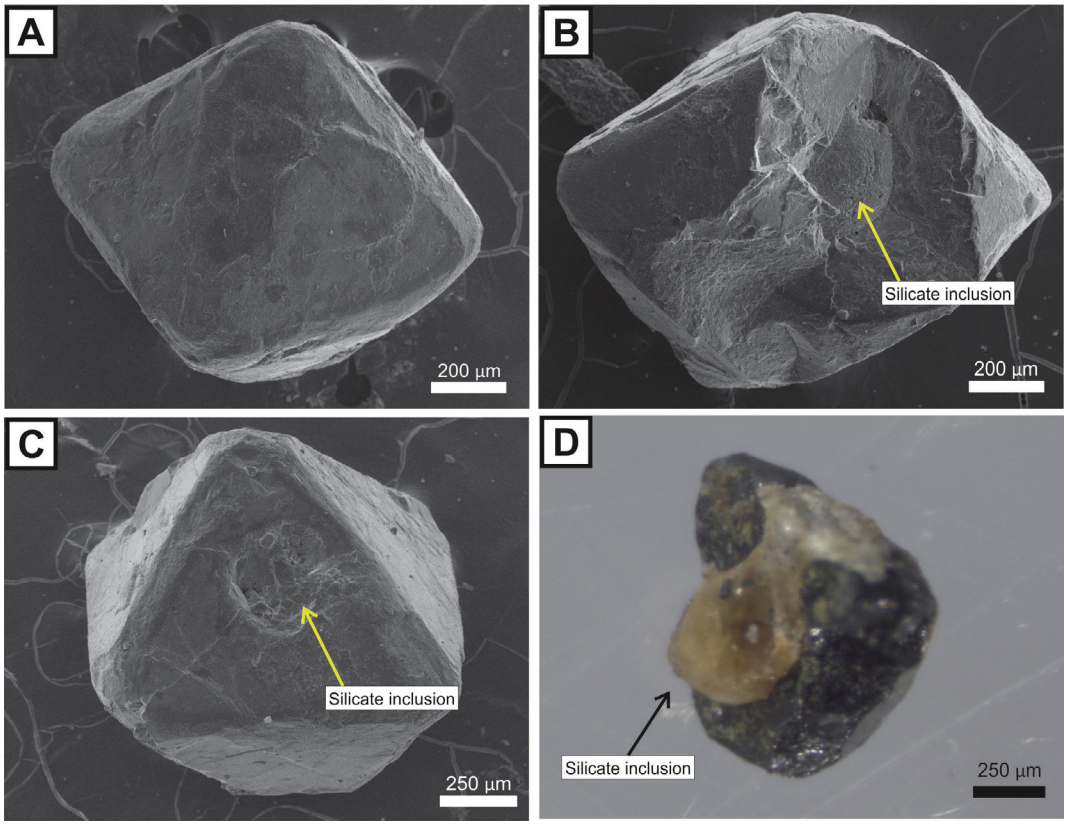

Fig. 6. Scanning Electron Microscope images of chromite crystals. (A) BSE mage of an euhedral chromite crystal. (B) BSE image of an euhedral chromite crystal showing one rounded silicate inclusion (up to 300 μm). (C) BSE image of chromite crystal with a partially-enclosed silicate inclusion. The silicate inclusion appears as a sub-circular shape in one face of the octahedral chromite crystal. (D) Photo (using a magnifying glass) of chromite grain enclosing a coalescent silicate inclusion (up to 300 μm). The inclusion shape indicates that the inclusion and interstitial minerals surrounding the chromite grain are connected.

inclusions (Fig. 5D). Both coarse chromite crystals and silicate inclusions show irregular shapes in the pegmatoidal chromitite (Fig. 5D), different from the euhedral crystals with rounded inclusions characteristic of the main chromitite. All three types of chromitites are cross-cut by fine grained amphibole-chlorite-carbonate veinlets (Fig. 5E). These veinlets do not appear to extensively affect the composition of chromite grains (i.e., no significant zonation or reaction border is observed).

Thin chromitites (<10 cm thick) are mainly hosted by noritic rocks of the Mafic Zone (UGC; Fig. 3). These chromitites are fine- to medium-grained chromite cumulates with intercumulus plagioclase and orthopyroxene (Fig. 4E). Chromite grains are euhedral and show many rounded silicate inclusions with well-developed inner rims (Fig. 5F). These inclusions consist of the same aggregate of fine-grained amphibole and chlorite crystals that replace the original intercumulus minerals in the main chromitite of the LGC. Locally, sulfide minerals occur at the bottom of the inclusions, facing the base of the chromitite layer (i.e., based on oriented thin sections; Fig. 5G).

5.2. Spatial analysis of silicate inclusions and their variation through the stratigraphy

Silicate inclusions and "atoll-like" structures are common features in chromite grains of the studied chromitites (Fig. 5). The three-dimensional shape of these inclusions and hosting crystals were described utilizing a SEM (Fig. 6). Chromite grains are euhedral with well-defined faces without any indication of reaction or reabsorption features (Fig. 6A). Inclusion-bearing crystals have the same morphology as inclusion-free crystals, except for the presence of predominantly rounded inclusions in the first (Fig. 6B). Inclusion-bearing chromite grains usually have the inclusions locked within the crystals, with no physical connection of the included silicates and outside matrix minerals. However, few silicate inclusions are connected with the outside matrix (Fig. 6C) where the inclusions are composed of the same silicate minerals that occur in the matrix of chromite grains (e.g., replaced plagioclase and/or orthopyroxene) (Fig. 6D).

The silicate inclusions show significant variations in shape, number and volume proportions within chromite crystals from chromitites of the LGC and UGC (Fig. 7). Chromite grains from the LGC commonly have just one large silicate inclusion (Fig. 7A). The thin pegmatoid chromitite (Fig. 3) has chromite crystals with larger silicate inclusions (up to 0.65 mm of diameter enclosed within chromite crystals of around 1 mm diameter) compare to all the studied samples (Fig. 7B). Upward in the stratigraphy, UGC are characterized by chromite grains with several small silicate inclusions (Fig. 7C).

6. Mineral chemistry

6.1. Orthopyroxene and plagioclase

Systematic studies of mineral chemistry of cumulus minerals from drill core LUFD-079 (i.e., orthopyroxene and plagioclase) were limited by metamorphic replacement of igneous minerals in several samples. Orthopyroxene was analysed in samples of orthopyroxenite and harzburgite from the Transition Zone and norite from the Mafic Zone, while plagioclase was just analysed in samples of norite from the Mafic Zone. Representative analyses of orthopyroxene and plagioclase are reported in Tables 1 and 2, respectively.

Orthopyroxene compositions range from En83.49 to En89.9 mol % through the top of the Transition Zone and the base of the Mafic Zone (Fig. 8). The cryptic variation of orthopyroxene shows a few reversals and relatively more fractionated compositions (En83.49 to En86.45 mol %) in the Transition Zone, whereas the compositions of orthopyroxene in norite of the Mafic Zone are more primitive (En89.0 to En89.84 mol %) (Fig. 8). Plagioclase compositions range from An76.61 to An83.20 mol % in the lower portion of the Mafic Zone. The plagioclase shows a consistent upward increase in An contents, indicating a reversed fractionation in the lower portion of the Mafic Zone (Fig. 8). Cryptic variations of orthopyroxene and plagioclase in drill core LUFD-079 are consistent with results described in previous studies of the Luanga Complex (Ferreira Filho et al., 2007; Mansur and Ferreira Filho, 2016). These results indicate common reversals within a general inversed fractionation trend for the Transition Zone and lower portion of the Mafic Zone.

6.2. Chromite

Chromite grains show alteration rims (Figs. 5 and 7) that are probably associated with different compositions. In order to evaluate the compositional variation in chromite grains, EMP analyses were performed on line transverses through 35 chromite crystals with different morphologies (Fig. 9 shows 4 representative line traverses), totaling ~700 analyses (Table A1). Investigated chromite crystals were separated into inclusion-free and inclusion-bearing crystals (see Table 3 and Table 4 for representative analyses from line traverses of inclusion-free and inclusion-bearing crystals, respectively). An outer alteration rim characterized by higher reflectance (see Fig. 9B) is common in both inclusion-free and inclusion-bearing crystals. They are variably thick and commonly continuous along fractures in extensively altered chromite crystals. Composition of chromite changes abruptly in this outer rim, becoming enriched in Fe^{3+} and Fe^{2+} (i.e., Fe^{3+}# up to 91) at the expense of Mg, Cr, Al. The outer alteration rim is easily recognized in petrographic studies and have highly different compositions compared with the core of the crystals. These rims were avoided in the systematic probe investigation and analyses are limited to a few line traverses (e.g., sample 49 in Table A1).

6.2.1. Line traverses through inclusion-free crystals

Inclusion-free crystals have a core-to-rim variation in composition (or concentric rim) that varies in thickness according to the modal percentage of chromite. Chromite crystals from massive

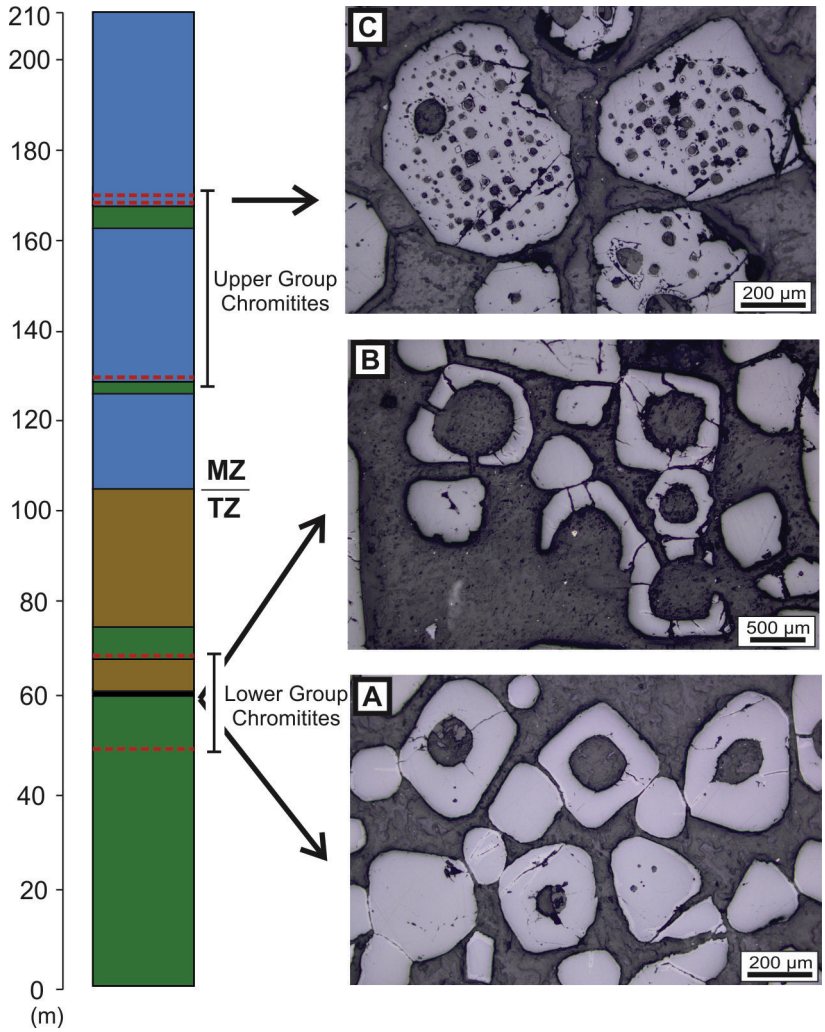

Fig. 7. Morphology of chromite grains in the stratigraphic section of drill hole LUFD-079. (A) Photomicrograph of representative inclusion-bearing chromite grains from chromitite of the Transition Zone. Chromite grains have one single rounded inclusion. (B) Photomicrograph of representative inclusion-bearing grains from the pegmatoid-textured chromitite. Chromite grains have one large inclusion or atoll-like texture. (C) Photomicrograph of representative inclusion-bearing chromite grains from thin chromitites of the Mafic Zone. Chromite grains have several inclusions. Note the characteristic sector zoning of inner rims adjacent to silicate inclusions. MZ = Mafic Zone; TZ = Transition Zone.

Table 1
Representative analyses of orthopyroxene.

Drill Hole	LUFD-079	LUFD-079	LUFD-079	LUFD-079	LUFD-079	LUFD-079	LUFD-079	LUFD-079	LUFD-079	LUFD-079
Depth (m)	63.75	78.92	101.5	176.4	176.4	176.4	188.8	205.57	205.57	205.57
Rock	Orthopyroxenite	Orthopyroxenite	Orthopyroxenite	Norite	Norite	Norite	Norite	Norite	Norite	Norite
SiO2 (wt.%)	54.96	55.43	54.87	54.95	54.96	55.03	55.17	55.23	55.41	55.43
TiO2	0.06	0.13	0.03	0.09	0.24	0.17	0.00	0.06	0.00	0.08
Al2O3	2.01	1.72	1.64	2.40	2.77	2.41	1.89	1.82	1.53	1.74
Cr2O3	0.46	0.69	0.47	0.79	0.51	0.60	0.40	0.36	0.29	0.40
FeO	10.18	9.10	10.33	7.04	7.25	6.91	7.43	6.90	7.05	7.02
MgO	31.85	32.03	29.31	33.15	33.76	33.60	33.73	34.44	34.66	34.61
MnO	0.22	0.14	0.12	0.05	0.03	0.15	0.17	0.19	0.18	0.12
NiO	0.20	0.18	0.15	0.16	0.18	0.17	0.17	0.13	0.15	0.15
CaO	0.67	1.10	2.65	1.42	0.77	0.76	1.01	1.07	1.03	0.71
Total	100.60	100.52	99.56	100.04	100.47	99.80	99.97	100.20	100.30	100.26
Normalization based on 24 oxygens										
Si (atoms%)	7.66	7.71	7.79	7.61	7.56	7.62	7.63	7.60	7.61	7.62
Al	0.33	0.28	0.20	0.38	0.43	0.37	0.30	0.29	0.24	0.28
Mg	6.61	6.65	6.21	6.84	6.93	6.94	6.96	7.06	7.10	7.09
Ca	0.10	0.16	0.40	0.21	0.11	0.11	0.15	0.15	0.15	0.10
Ti	0.00	0.01	0.00	0.00	0.02	0.01	0.00	0.00	0.00	0.00
Cr	0.05	0.07	0.05	0.08	0.05	0.06	0.04	0.03	0.03	0.04
Fe^{2+}	1.18	1.05	1.22	0.81	0.83	0.80	0.86	0.79	0.81	0.80
Ni	0.01	0.01	0.01	0.01	0.01	0.01	0.01	0.0	0.01	0.01
Mn	0.02	0.01	0.01	0.00	0.00	0.01	0.02	0.02	0.02	0.01
Total	16.00	16.00	15.92	15.99	15.97	15.97	16.00	16.00	16.00	16.00
En (%)	84.80	86.26	83.49	89.36	89.25	89.66	89.00	89.89	89.75	89.78

Table 2
Representative analyses of plagioclase.

Drill Hole	LUFD-079	LUFD-079	LUFD-079	LUFD-079	LUFD-079	LUFD-079
Depth (m)	132.2	132.2	161	161	188.8	188.8
Rock	Norite	Norite	Norite	Norite	Norite	Norite
SiO_2 (wt%)	49.06	48.77	48.12	47.85	47.60	47.31
Al_2O_3	32.78	32.82	33.07	33.45	33.65	33.48
FeO	0.25	0.23	0.24	0.19	0.22	0.25
CaO	15.44	15.90	16.18	16.55	16.65	16.87
Na_2O	2.59	2.41	2.45	2.18	2.08	2.02
K_2O	0.03	0.05	0.04	0.05	0.07	0.03
Total	100.15	100.17	100.10	100.27	100.25	99.96
Normalization based on 8 oxygens						
Si (atoms %)	2.24	2.23	2.20	2.19	2.18	2.17
Al	1.76	1.77	1.79	1.80	1.82	1.81
Fe^{2+}	0.01	0.01	0.01	0.01	0.01	0.01
Ca	0.75	0.78	0.79	0.81	0.82	0.83
Na	0.23	0.21	0.22	0.19	0.18	0.18
K	0.00	0.00	0.00	0.00	0.00	0.00
Total	5.00	5.00	5.01	5.01	5.01	5.01
An	76.61	78.22	78.32	80.53	81.28	82.07

chromitites (i.e., >50 vol% of chromite) have thinner concentric rims compared with chain-textured and disseminated chromitites (i.e., <50 vol% of chromite). Line traverses through inclusion-free crystals (Fig. 9A and B) show significant progressive core to rim changes in Mg# (i.e., a Mg-Fe core-rim zoning). The core of the crystals has higher Mg and lower Fe^{2+} contents than the rims, resulting in an up to 40% difference in Mg# across a chromite crystal. Difference in Mg# from core to rim progressively decreases for chromitites with higher amount of intercumulus minerals, as illustrated by line traverses through chromite crystals from massive (Fig. 9A), chain-textured (Fig. 9B) and disseminated (Fig. 9C) chromitites. This feature (i.e., the progressively lower difference in Mg# for chromitites with higher amounts of intercumulus minerals) is matched with progressively lower Mg# in the core of chromite grains. Significant differences in Mg# of chromite crystals suggest extensive Mg and Fe^{2+} exchange, a subject to be addressed in the discussion of this study. The Cr#, Al# and Fe^{3+}# are constant in line traverses through different types of chromite crystals (Fig. 9A–C), except for few analyses located in the outer bright colored rim in some crystals (not analysed for line traverses represented in Fig 9A–C). This feature indicates that the suggested extensive exchange between divalent cations in chromite crystals (i.e., Mg and Fe^{2+}) does not affect trivalent cations (i.e., Cr, Al and Fe^{3+}). Zn contents are commonly low and many results are below or close to detection limits of our analyses, resulting in highly scattered profiles. Nevertheless, Zn contents are consistently higher in the outer zone of the rims (see Table 3 for representative analyses of Zn in one line traverse).

6.2.2. Line traverses through inclusion-bearing crystals

Inclusion-bearing crystals (Figs. 5F, G and 7) have an outer alteration rim, similar to the one described for inclusion-free crystals, and a variably developed rim adjacent to the silicate inclusions (Fig. 9D). The latter, designated inner rim, has a distinctive morphology consisting of rounded contacts with the silicate inclusion and a characteristic sector zoning following the octahedral form of the hosting chromite crystals (Fig. 9D). The existence and/or extent of the inner rim do not have any systematic relation with the size of host chromite crystal and silicate inclusion, the number of inclusions, or the chromite modal percentage and texture of the chromitite. Line traverses through inclusion-bearing crystals (Fig. 9D) indicate significant compositional changes close to silicate inclusions. Compared to the host chromite, compositions within the rims adjacent to silicate inclusions have higher Cr#, lower Al# and Mg# and similar Fe^{3+}# (Fig. 9D). These relative compositional changes are described for all studied rims regardless the size and/or composition of the host chromite.

6.2.3. Cryptic variation of chromite

Line traverses across chromite crystals of several chromitites from drill core LUFD-079 indicate that chromite compositions are highly variable for each sample. Compositional variation occurs within a single grain (i.e., zoning) as well as when different grains from the same sample are compared. The study of cryptic variation in chromite through drill core LUFD-079 (Fig. 8) includes just compositions obtained in homogenous core of inclusion-free chromite crystals from chain-textured or massive chromitites. These compositions are likely to be close to primary crystallization compositions and largely reduce the variability resulting from zoned crystals.

Chromite compositions from chromitites throughout drill core LUFD-079 indicate an increase in Al# along with a decrease in Cr# (Fig. 8). Cr# and Al# of LGC (including samples from the main chromitite), respectively 45–54 and 32–44, are distinctively different from those obtained in UGC, respectively 36–42 and 52–58. The Fe^{3+}# follows the Cr# and decrease from LGC (6–19) to UGC (1–9). The Mg# in chromite is largely controlled by textural features of chromite and the modal percentage of chromite, as indicated in the description of line traverses. Mg# are low and close to ~20 for all chromitites, except for higher and highly variable values (30–66) for samples of the main chromitite. The low values of Mg# obtained for most chromitites are likely to result from later alteration processes and, therefore, not useful as an indication of magmatic evolution.

Chromite compositions from samples of the main chromitite do not provide any significant base-to-top compositional trend (Fig. 10). Cr# and Al# in chromite crystals show negative correlation and a limited compositional range, respectively 47–51 and 36–42, except for the unusually Fe^{3+} rich (8–15) and Cr-poor (45–50) uppermost sample. Highly variable Mg# (22–62) are likely to result from heterogeneous effects of alteration processes, as previously described for other chromitites from drill core LUFD-079.

7. Discussion

7.1. Magmatic compositions of chromite

The extensive database of chromite analyses (~700 analyses) for chromitites of the Luanga Complex obtained in this study indicates a large range of compositions. Two common projections of

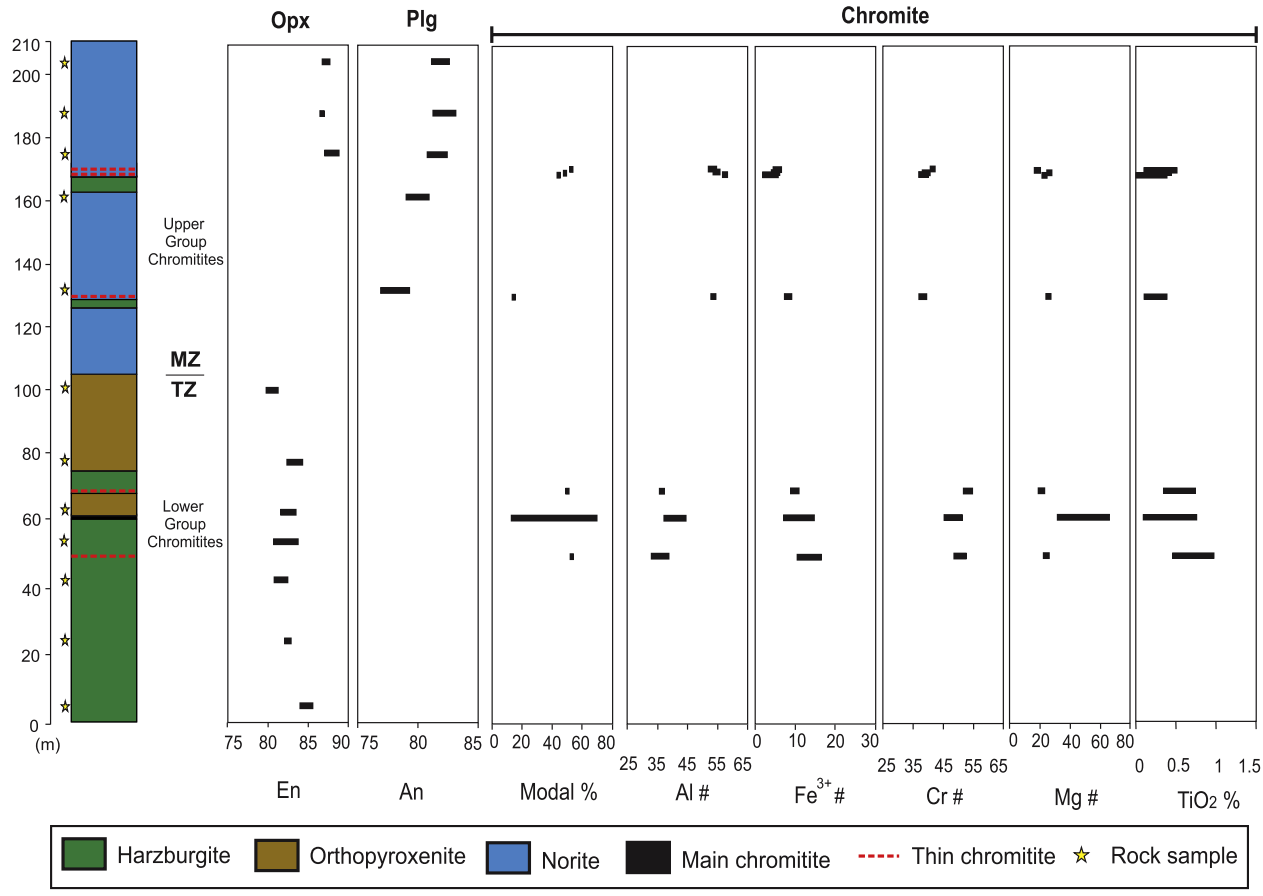

Fig. 8. Compositional variations of orthopyroxene (Opx), plagioclase (Plg) and chromite throughout drill core LUFD-079. Orthopyroxene and plagioclase compositions are indicated as enstatite (En) and anorthite (An) contents (mol.%), respectively. Chromite compositions are indicated as Al# = 100Al/(Al + Cr + Fe^{3+}), Cr# = 100Cr/(Cr + Al + Fe^{3+}), Fe^{3+}# = 100Fe^{3+}/(Fe^{3+} + Cr + Al), Mg# = 100 Mg/(Mg + Fe^{2+}) and TiO_2 (wt%). Modal% indicates the chromite percentage of each chromitite. The black bar indicates the variation in composition for each sample. MZ = Mafic Zone; TZ = Transition Zone.

the spinel compositional prism, the triangular Cr-Al-Fe^{3+} plot (Fig. 11) and the plot of Fe^{2+}/(Mg + Fe^{2+}) vs Cr/(Cr + Al) (Fig. 12), are used to illustrate the compositional variation of chromite in chromitites. Results indicate that LGC have distinctively higher Cr# compared with UGC. The upward decrease of Cr# in chromitites of the Luanga Complex matches the fractionation of the magma from ultramafic cumulates (olivine and/or orthopyroxene cumulates) in the Transition Zone to plagioclase-bearing cumulates in the Mafic Zone (Fig. 8). Our results also indicate that compositions of chromite from the UGC are distinctively different from those hosted in chromitites from continental layered intrusions (Fig. 12). While most chromitites in continental layered intrusions are located within ultramafic cumulates, our results for the UGC add another case for the few examples of chromitites hosted within mafic cumulate (e.g., Rum layered intrusion, Henderson, 1975; Upper Group chromitites of the Bushveld Complex, Eales and Reynolds, 1986). Due to extensive Fe^{+2} and Mg compositional variation in chromite, our data is highly scattered in a Fe# vs Cr# plot (Fig. 12). Therefore, typical trends indicating either a positive correlation between Fe# (or otherwise a negative correlation if Mg# is plotted) and Cr# (known as the Cr-Al trend by Barnes and Roeder, 2001), or a negative correlation (known as the Rum trend by Barnes and Roeder, 2001) are not obvious for chromitites from the Luanga Complex (Fig. 12). Nevertheless, the very low Cr# of the UGC and the abrupt upward decrease in Cr# from the LGC to the UGC are remarkable compositional features. Lower Cr# in the UGC results from the increase in Al at the expense of Cr and some Fe^{3+} (Figs. 8 and 12). The upward decrease in the Cr# through a layered intrusion has been ascribed to the depletion of Cr in the melt during fractionation (Irvine, 1977; Hulbert and Von Gruenewaldt, 1985). However, the content of TiO_2 in chromite from chromitites of the Luanga Complex (Fig. 8) does not show an upward increase as expected for progressively more fractionated magmas. It should also be noted that chromite in the Upper Group of the Bushveld Complex chromitites have higher Cr# compared with chromite in the underlying Middle Group chromitites, a feature interpreted as the result of reduced Al_2O_3 activity by the appearance of cumulus plagioclase in cumulates hosting the Upper Group chromitites (Eales and Marsh, 1983; Naldrett et al., 2009). The previous discussion suggests that the unusual composition of the UGC chromitites are not satisfactory explained by models and processes indicated for chromitites from other locations. We suggest that compositions of the UGC chromite may be linked to petrological processes associated with peridotites underlying each chromitite, an issue addressed in the following discussion.

7.2. Petrological implications of the stratigraphic distribution of chromitites

As commonly described in layered intrusions, chromitites in the Luanga Complex occur in specific stratigraphic intervals with distinct petrological characteristics. Chromitites occur mainly in the upper portions of the Transition Zone and through the immediate contact with the Mafic Zone (Fig. 2C), a stratigraphic interval consisting of several cyclic units interpreted as the result of successive influxes of parental magma (Mansur and Ferreira Filho, 2016). Dif-

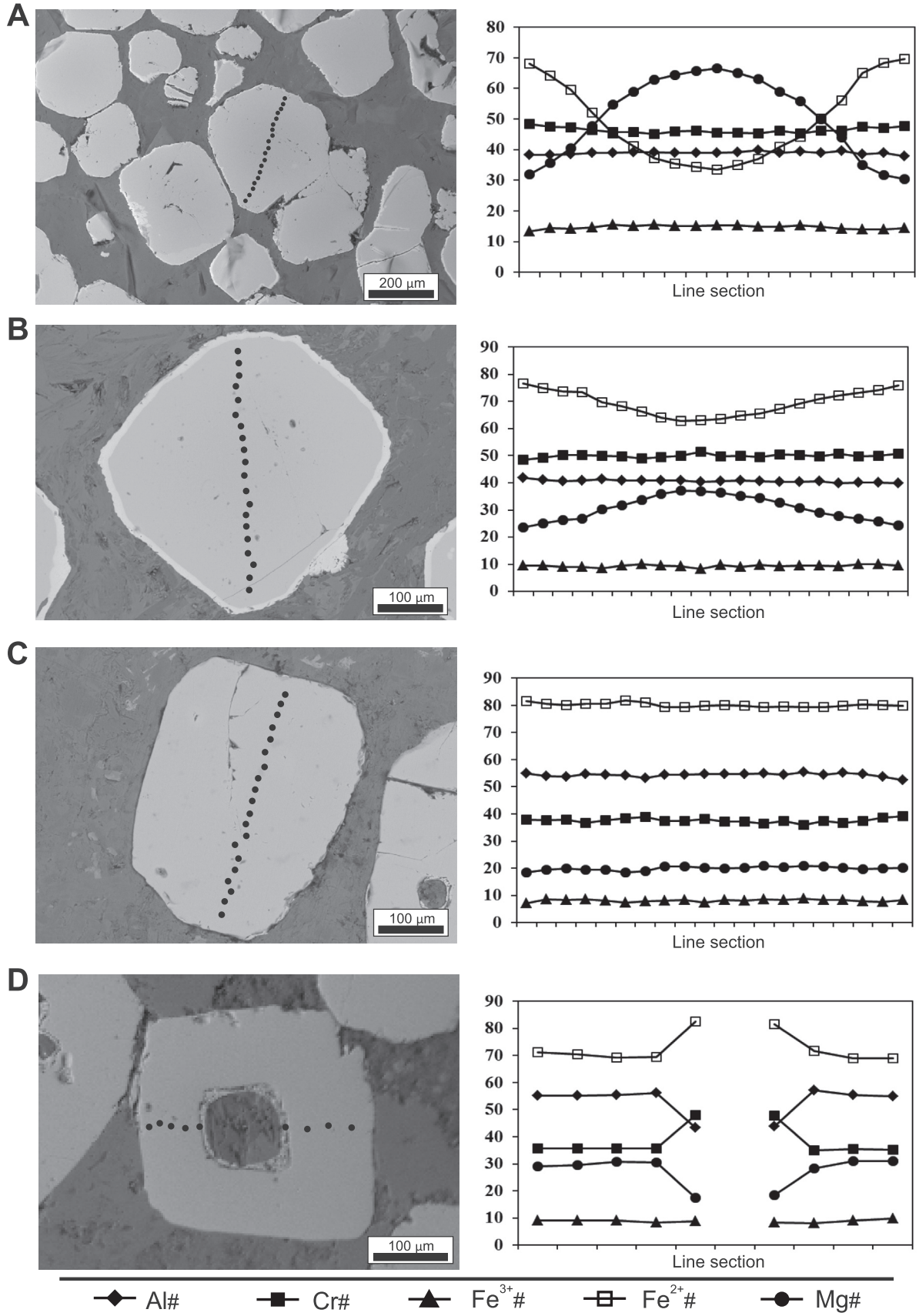

Fig. 9. Back-scattered images of chromite grains analysed in line transverses in EMP and plots of the results. (A) Massive chromitite from the main chromitite of the Transition Zone. (B) Chain-textured chromitite from the main chromitite of the Transition Zone. (C) Disseminated chromitite from the main chromitite of the Transition Zone. (D) Inclusion-bearing chromite grain from a thin chromitite of the Mafic Zone.

Table 3
Representative analyses of chromite from a line transverse across an inclusion-free chromite grain.

Drill Hole	LUFD-79	LUFD-79	LUFD-79	LUFD-79	LUFD-79	LUFD-79	LUFD-79	LUFD-79	LUFD-79	LUFD-79
Depth	62.4	62.4	62.4	62.4	62.4	62.4	62.4	62.4	62.4	62.4
Texture	Mass.	Mass.	Mass.	Mass.	Mass.	Mass.	Mass.	Mass.	Mass.	Mass.
SiO_2 (wt%)	<0.01	<0.01	<0.01	<0.01	<0.01	<0.01	<0.01	<0.01	<0.01	<0.01
TiO_2	0.77	0.24	0.64	0.36	0.67	0.42	0.53	0.49	0.45	0.18
Al_2O_3	20.63	20.99	22.37	22.79	23.05	22.48	22.80	22.22	21.22	20.82
Fe_2O_3	7.43	9.10	7.64	7.78	7.48	7.75	7.16	7.52	8.14	8.28
FeO	24.39	22.08	20.13	16.83	17.13	16.93	18.86	20.04	24.31	24.45
MnO	0.24	0.36	0.14	0.16	0.21	0.06	0.20	0.32	0.31	0.32
MgO	6.41	7.79	10.03	12.08	12.14	12.07	10.88	9.85	6.63	6.15
CaO	<0.01	<0.01	<0.01	<0.01	0.02	<0.01	0.03	<0.01	0.04	<0.01
Cr_2O_3	36.58	36.77	38.16	39.27	38.8	39.67	39.15	38.73	37.34	37.19
V_2O_3	0.15	0.21	0.17	0.11	0.20	0.20	0.15	0.11	0.10	0.18
ZnO	0.37	0.26	0.09	0.06	0.03	0.17	0.13	0.16	0.42	0.52
NiO	0.24	0.23	0.24	0.24	0.23	0.28	0.22	0.22	0.26	0.21
Total	97.22	98.02	99.62	99.67	99.96	100.03	100.10	99.68	99.23	98.30
Number of cations per 32 oxygen ions										
Si (atoms %)	<0.01	<0.01	<0.01	<0.01	<0.01	<0.01	<0.01	<0.01	<0.01	<0.01
Ti	0.15	0.05	0.12	0.07	0.12	0.08	0.10	0.09	0.09	0.04
Al	6.47	6.47	6.66	6.68	6.72	6.57	6.7	6.62	6.51	6.48
Fe^{3+}	1.49	1.79	1.45	1.45	1.39	1.45	1.34	1.43	1.60	1.65
Fe^{2+}	5.43	4.83	4.25	3.50	3.55	3.51	3.94	4.24	5.30	5.40
Mn	0.05	0.08	0.03	0.03	0.04	0.01	0.04	0.07	0.07	0.07
Mg	2.54	3.04	3.77	4.47	4.48	4.47	4.05	3.71	2.57	2.42
Ca	<0.01	<0.01	<0.01	<0.01	<0.01	<0.01	0.01	<0.01	0.01	<0.01
Cr	7.70	7.60	7.62	7.72	7.59	7.78	7.72	7.74	7.69	7.76
V	0.03	0.04	0.03	0.02	0.04	0.04	0.03	0.02	0.02	0.04
Zn	0.07	0.05	0.02	0.01	0.01	0.03	0.02	0.03	0.08	0.10
Ni	0.05	0.05	0.05	0.05	0.05	0.06	0.04	0.04	0.05	0.04
Total	24	24	24	24	24	24	24	24	24	24
Cr#	49.16	47.93	48.43	48.69	48.34	49.24	48.97	49.01	48.68	48.87
Mg #	31.89	38.61	47.03	56.12	55.81	55.97	50.69	46.71	32.70	30.95
Fe^{3+}#	9.51	11.29	9.23	9.18	8.87	9.16	8.52	9.06	10.10	10.35
Al#	41.33	40.78	42.33	42.13	42.80	41.60	42.51	41.93	41.22	40.78

ferent models were proposed to explain the common association of chromitites and cyclic units. They include, among others, the mixing of an injection of primitive magma with a more fractionated magma residing in the magma chamber, thus causing chromite to be the sole liquidus mineral (e.g., Irvine, 1977), chromite crystallization in a staging magma chamber then injection of the chromite-bearing slurry (e.g., Mondal and Mathez, 2007; Voordouw et al., 2009) and the result of slumping of semi-consolidated cumulates in a chromite-rich slurry (e.g., Maier and Barnes, 2008). It is not the aim of this paper to discuss the processes that lead to the accumulation of chromite-rich layers, a highly controversial subject (see Mondal and Mathez, 2007 and Naldrett et al., 2012 for reviews and references). We rather want to focus on possible petrological implications provided by the stratigraphic sequence associated with chromitites in the Mafic Zone (Fig. 3). Thin chromitites hosted by noritic rocks are always preceded by a thin layer of harzburgite located 15–20 cm below each chromitite layer (Fig. 4C–E). Because this unusual stratigraphic association of harzburgite and chromitite is consistently repeated, a petrological link of harzburgite layers and chromitites located above them is suggested. Thin chromitites closely associated with peridotite-troctolite are also reported in the Rum Complex (O'Driscoll et al., 2010). Although chromitites in the Rum Complex occur mainly at the base of several peridotite-troctolite cyclic units, thin chromitites also occur a few centimeters away from the basal peridotite. O'Driscoll et al. (2010) suggested that chromitites were formed by *in situ* crystallization following assimilation of troctolitic cumulate by a new influx of primitive magma at the crystal mush-magma interface. The authors' also suggested that chromitites located above the unit boundaries resulted from coeval syn-magmatic deformation of the crystal mush. This interpretation may be also applied for chromitites hosted in noritic rocks of the Luanga Complex. When the new influx of primitive magma assimilated norite the concentration (and thus activity) of Al_2O_3 should have increased. The relatively lower Cr# and Fe^{+3} of chromite in the UGC may result from an increase in Al_2O_3 activity right in the crystal mush-primitive magma interface, just preceding the first appearance of liquidus plagioclase. This suggestion follows O'Driscoll et al. (2010) idea that unusually aluminous composition of chromite in the Rum Complex resulted from high Al_2O_3 content of hybrid liquids originated from assimilation of plagioclase-rich cumulate from a picritic magma.

7.3. Compositional zonation in chromite grains and its implications for the interpretation of chromite compositions

Our results indicate that extensive compositional variation occurs in different scales, as indicated by large variation obtained in analyses of one chromitite (Figs. 11B and 12B) or even within a chromite crystal (Figs. 11C and 12C). Compositional traverses in chromite crystals from several chromitites of the Luanga Complex indicate three distinct types of rim or compositional zoning: i) an outer alteration rim, ii) a Mg-Fe core-rim zoning, iii) an inner rim adjacent to silicate inclusions. Distinct textures and compositions of these three types of rim or zoning suggest that they originated from different processes.

An outer alteration rim characterized by higher reflectance (see Fig. 9B and photomicrographs in Sack and Ghiorso, 1991) is common in chromite crystals from chromitites overprinted by metamorphism, especially under lower to intermediate grades of the regional metamorphism (i.e., up to amphibolite facies) (e.g., Evans and Frost, 1975; Sack and Ghiorso, 1991; Liipo et al., 1995). This alteration is also common in chromite crystals in serpentinized and/or hydrothermally altered mafic–ultramafic rocks

Table 4
Representative analyses of chromite from a line transverse across an inclusion-bearing chromite grain.

Drill Hole	LUFD-79	LUFD-79	LUFD-79	LUFD-79	LUFD-79	LUFD-79	LUFD-79	LUFD-79	LUFD-79
Depth	169.30	169.30	169.30	169.30	169.30	169.30	169.30	169.30	169.30
SiO_2 (wt%)	<0.01	<0.01	<0.01	<0.01	0.06	0.07	0.06	<0.01	<0.01
TiO_2	0.21	0.10	0.03	0.23	0.15	0.18	0.00	0.00	0.19
Al_2O_3	28.68	29.07	29.32	29.75	21.36	21.71	30.01	29.27	28.90
Cr_2O_3	27.57	28.07	28.07	28.19	35.34	35.27	27.42	27.96	27.51
Fe_2O_3	7.39	7.57	7.56	6.94	6.77	6.43	6.54	7.72	8.14
FeO	25.39	25.66	25.08	25.45	28.15	27.65	25.72	24.86	24.75
MnO	0.32	0.31	0.37	0.28	0.52	0.64	0.44	0.30	0.36
MgO	5.80	6.02	6.27	6.27	3.33	3.51	5.68	6.28	6.23
CaO	<0.01	<0.01	<0.01	<0.01	<0.01	<0.01	<0.01	<0.01	0.03
NiO	0.12	0.19	0.15	0.13	0.06	0.00	0.02	0.17	0.23
ZnO	0.94	0.53	0.75	0.92	0.74	0.97	1.31	0.94	1.04
V2O3	0.15	0.06	0.11	0.10	0.13	0.12	0.11	0.09	0.13
Total	95.84	96.82	96.96	97.58	95.97	95.92	96.67	96.83	96.70
Number of cations per 32 oxygen ions									
Si (atoms %)	<0.01	<0.01	<0.01	<0.01	0.02	0.02	0.02	<0.01	<0.01
Ti	0.04	0.02	0.01	0.04	0.03	0.04	0.00	0.00	0.04
Al	8.78	8.79	8.84	8.91	6.86	6.96	9.07	8.83	8.75
Fe^{3+}	1.44	1.44	1.43	1.33	1.39	1.32	1.26	1.45	1.56
Fe^{2+}	5.52	5.51	5.36	5.41	6.42	6.29	5.52	5.32	5.31
Cr	5.66	5.69	5.68	5.66	7.61	7.58	5.56	5.66	5.58
Mn	0.07	0.07	0.08	0.06	0.12	0.15	0.09	0.06	0.08
Mg	2.25	2.30	2.39	2.37	1.35	1.42	2.17	2.40	2.38
Ca	<0.01	<0.01	<0.01	<0.01	<0.01	<0.01	<0.01	<0.01	0.01
Ni	0.02	0.04	0.03	0.03	0.01	0.00	0.00	0.03	0.05
Zn	0.18	0.10	0.14	0.17	0.15	0.19	0.25	0.18	0.20
V	0.03	0.01	0.02	0.02	0.03	0.03	0.02	0.02	0.03
Total	24.00	23.98	23.98	24.00	24.00	24.00	24.00	23.97	23.99
Al^{3+} ratio	55.27	55.20	55.42	56.03	43.25	43.88	57.07	55.39	55.03
Cr^{3+} ratio	35.64	35.75	35.60	35.62	48.00	47.82	34.98	35.49	35.14
Fe^{3+} ratio	9.09	9.05	8.97	8.35	8.75	8.30	7.94	9.11	9.83
Fe^{2+} ratio	71.07	70.52	69.19	69.48	82.60	81.54	71.74	68.95	69.03
Mg^{2+} ratio	28.93	29.48	30.81	30.52	17.40	18.46	28.26	31.05	30.97

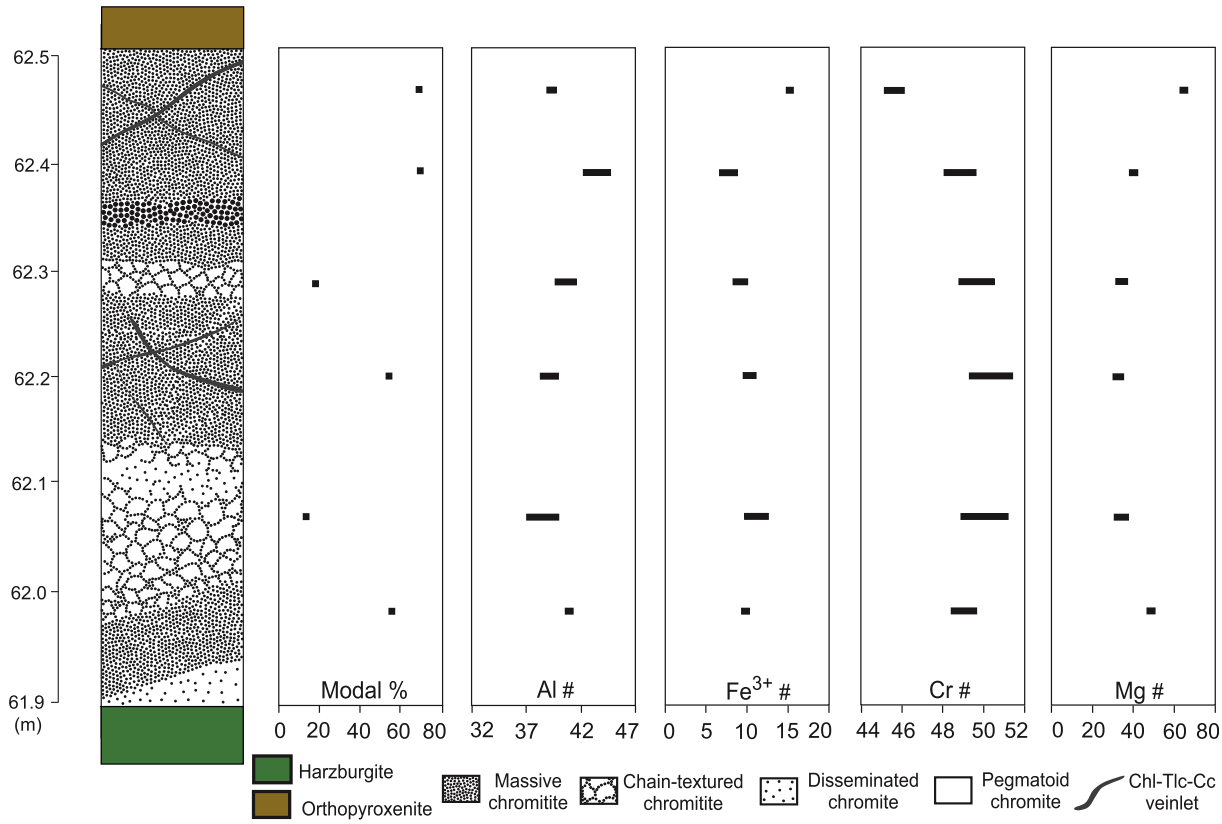

Fig. 10. Compositional variations of chromite throughout the main chromitite of the Transition Zone (see stratigraphic section in Fig. 3 for orientation). Chromite compositions are expressed in terms of Al# = 100Al/(Al + Cr + Fe^{3+}), Cr# = 100Cr/(Cr + Al + Fe^{3+}), Fe^{3+}# = 100Fe^{3+}/(Fe^{3+} + Cr + Al) and Mg# = 100 Mg/(Mg + Fe^{2+}). Modal% indicates the chromite percentage of each sample. The black bar indicates the variation for each sample.

(e.g., Barnes and Roeder, 2001; Mukherjee et al., 2010, 2015). The composition of chromite in samples of the Luanga Complex changes abruptly in the outer rim, becoming enriched in Fe^{3+} and Fe^{2+} at the expense of Mg, Cr, Al, thus moving toward the magnetite apex on the spinel prism. The formation of the outer rim is probably related to the metamorphic replacement of the primary mineralogy of the Luanga Complex. This interpretation is supported by the occurrence of larger outer rims in chromite associated with extensively replaced rocks. While chromite grains are commonly completely altered to magnetite-ferrichromite in extensively replaced rocks, chromite enclosed in relicts of olivine or orthopyroxene have just minor alteration along fractures. The common increase in Zn contents close to the outer rim of chromite in the Luanga Complex chomitites may be associated with the metamorphism, an explanation proposed for elevated Zn contents in chromite hosted in komatiites metamorphosed under greenshist to lower amphibolite grade (Barnes, 2000).

The Mg-Fe zoning in chromite crystals has a strong correlation with the modal percentage of chromite in a given layer (Fig. 9A–C). This is indicated by thinner concentric rims in chromite crystals from massive chromitites (i.e., >50 vol% of chromite) compared with chain-textured and disseminated chromitites (i.e., <50 vol% of chromite), and has been described in several studies of chromitites (e.g., Danyushevsky et al., 2000; Marques and Ferreira Filho, 2003; Spandler et al., 2005). The Mg-Fe zoning in chromite crystals results from significant core-to-rim differences in Fe^{2+} and Mg contents with none to minor differences in Fe^{3+}, Al and Cr contents. The progressive core-to-rim decrease in Mg# of chromite crystals may result either from an evolving melt composition during crystallization, or by subsolidus exchange of Fe^{2+} and Mg between chromite and coexisting silicates during slow cooling of the intrusion. The first option is favored by the progressive fractionation of the trapped intercumulus liquid coexisting with cumulus chromite (e.g., Henderson and Wood, 1981; Roeder and Campbell, 1985). However, the fractionated trapped melt should become enriched in TiO_2 and Fe^{3+} and therefore, a negative correlation of Mg# and Fe^{3+}# along with TiO_2 contents would be expected for Mg-Fe zoned chromite crystals. Because these correlations do not occur in the Mg-Fe zoned crystals of the Luanga Complex (Fig. 9), the first option is not an appropriate interpretation. The second option demands an extensive exchange between divalent cations hosted in tetrahedral sites in chromite crystals (i.e., Mg and Fe^{2+}) and coexisting silicates. This extensive exchange would not be accompanied with exchange between trivalent cations hosted in octahedral sites (i.e., Cr, Al and Fe^{3+}) in chromite and coexisting silicates due to their lower diffusion rates (Sack and Ghiorso, 1991). The second option has been proposed as an explanation for Fe^{2+} and Mg variation across chromite grains in chromitites (e.g., Danyushevsky et al., 2000; Spier and Ferreira Filho, 2001; Spandler et al., 2005), and provides an appropriate interpretation for Mg-Fe zoned chromite crystals of the Luanga Complex.

Inclusion-bearing chromite crystals have the same Mg-Fe zoning but also show additional inner rims adjacent to the silicate inclusions (Fig. 9D). The chromite composition adjacent to the silicate inclusion (i.e., in the inner rim) have higher Cr#, lower Mg# and Al#, and similar Fe^{3+}# (Fig. 9D), possibly due to crystallization from a progressively more fractionationed liquid trapped in the chromite crystal (i.e., following the process suggested for progressive fractionation of the trapped intercumulus liquid by Henderson and Wood, 1981). Borisova et al. (2012) describe chromites with similar compositional variation in coronas adjacent to silicate inclusions from the Oman ophiolite. Based on the hydrous

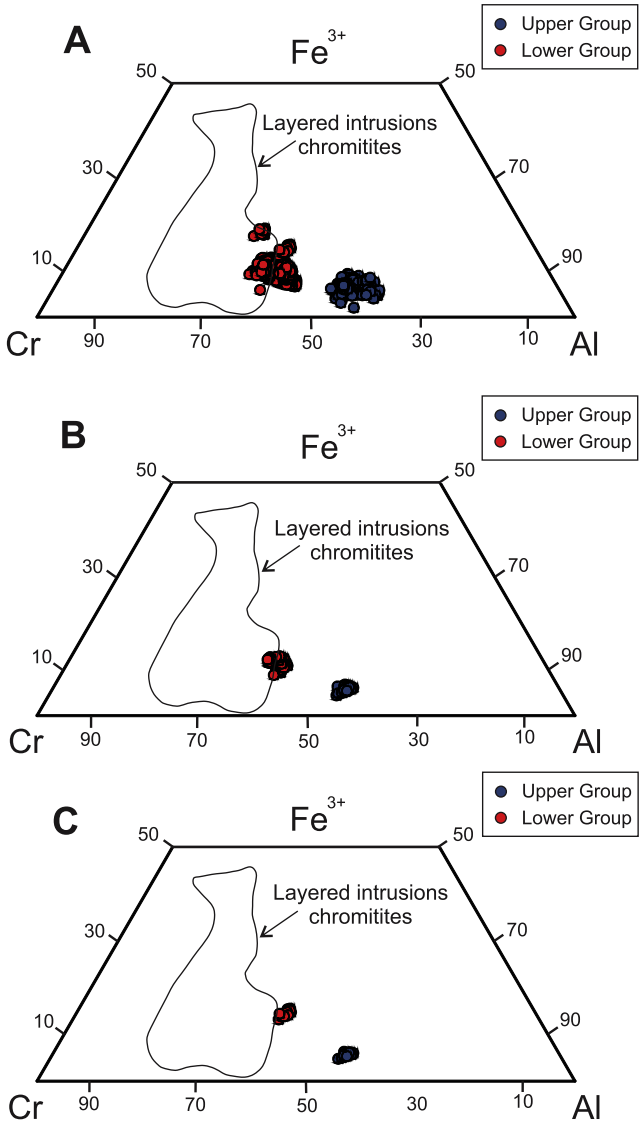

Fig. 11. Ternary plot (Fe^{3+}#-Cr#-Al# of chromites from chromitites of the Luanga Complex. (A) Chromite analyses from all chromitites investigated. (B) Analyses of chromite from one chromitite of the Transition Zone (Lower Group) and one of the Mafic Zone (Upper Group). (C) Analyses of chromite from a line traverse of one representative chromite crystal from the chromitites indicated in (B). The field of chromite compositions in layered intrusions is from Barnes and Roeder (2001).

Na-Cl-rich composition of the melt inclusions, the authors proposed a subsolidus process for the origin of the coronas in chromite from the Oman ophiolite, suggesting that metamorphic processes induced higher Cr# in chromite close to the hydrous silicate inclusions. Because silicate inclusions in the Luanga Complex are eventually connected to intercumulus minerals, and no evidence for hydrous Na-Cl melt inclusions exists, such a hydrothermal-metamorphic process is not favored for the inner rim coronas described in our study. In particular, reaction of Cr-spinel with intercumulus liquid, as suggested for the inner rim coronas of the Luanga Complex, results in both divalent (Fe^{2+} and Mg) and trivalent (Cr, Al, Fe,) cation exchange. On the other hand, subsolidus reaction of Cr-spinel and intercumulus silicates, as suggested for the Fe-Mg zoning, results mainly in exchange of divalent cations.

Our results indicate that chromite compositions from chromitites of the Luanga Complex (Figs. 11 and 12) have their primary cumulus composition extensively modified by postcumulus magmatic processes. Although distinct primary magmatic compositions are indicated by different Cr# for chromites from the Transition Zone and Mafic Zone, the extensive variation of Mg#, even for a single chromite crystal, indicates that the compositional field of the Luanga Complex chromitites are not entirely primary magmatic. Due to the indicated modification of primary magmatic compositions, it is critical to determine what range of compositions of the Luanga Complex chromites represents the closest composition of original cumulus chromite. These are the compositions useful for defining magmatic trends and/or comparison with other layered intrusions. Mass balance arguments are commonly used to indicate that massive chromitites with >70 vol% chromite are likely to preserve its original igneous compositions because there are few other phases available for element exchange (e.g., Eales and Reynolds, 1986). This reasoning was used in several studies of chromitites (e.g., Bacuri Complex, Spier and Ferreira Filho, 2001; Ipueira-Medrado Sill, Marques and Ferreira Filho, 2003), but is not appropriate for chromitites of the Luanga Complex, where modal compositions rarely exceed 70 vol%. Our results suggest, in fact, that just the compositions from analyses in the very core of chromite from massive portions of the main chromitite (e.g., Fig. 9A) represent compositions close to original cumulus compositions of the Luanga Complex. None of the other analyses represent cumulus compositions. These altered compositions represent >90% of the analyses of this study, including all analyses of chromite from chromitites of the Mafic Zone. The range of chromite compositions likely to represent compositions close to primary cumulus chromite for chromitites of the Transition Zone, as well as the range of Fe^{+2}-Mg exchange, is indicated in Fig. 13. Chromite compositions likely to represent compositions close to primary cumulus chromite are limited to analyses with high Mg# in the core of chromite from massive portions of the main chromitite (as indicated in Fig. 9A).

The extensive modification of primary cumulus composition of chromite, indicated in our study for the Luanga Complex, is likely to be common in non-massive chromitites (i.e., <70 vol% chromite), and the rule for disseminated chromites in mafic intrusions. Therefore, the common use of spinel compositions as a petrogenetic indicator for mafic intrusions (e.g., Sack and Ghiorso, 1991; Power et al., 2000; Barnes and Roeder, 2001) should be considered with caution and always supported by extensive petrographic/analytical investigation of post-magmatic alteration.

7.4. Why different types of inclusion-bearing chromite crystals are formed?

Silicate inclusions of distinct types are common in chromitites through the stratigraphy of the Luanga Complex (Figs. 5, 6 and 7). Different models have been proposed to explain the formation of silicate inclusions in chromite (e.g., Augé, 1987; Ballhaus and Stumpfl, 1986; Hulbert and Von Gruenewaldt, 1985; Li et al., 2005; Lorand and Cottin, 1987; Lorand and Ceuleneer, 1989; Roeder et al., 2001; Spandler et al., 2005). It is beyond the scope of this article to enter into a thorough discussion of the mechanisms of formation of these inclusions, and just a parallel of our observation and available models is considered in here.

Based on the size and number of inclusions, the inclusion-bearing chromite grains of the Luanga Complex split into two groups. LGC commonly have chromite crystals with just one large inclusion (Fig. 7A), while UGC consist mainly of chromite grains with several small inclusions (Fig. 7C). Both groups show inclusion coalescence (Figs. 5E and 6D), minor accumulation of sulfides (consisting mainly of variable proportions of pyrrhotite and pentlandite) at the bottom of inclusions (Fig. 5G) and rounded shapes (Figs. 5 to 7). Processes that lead to chromite recrystallization

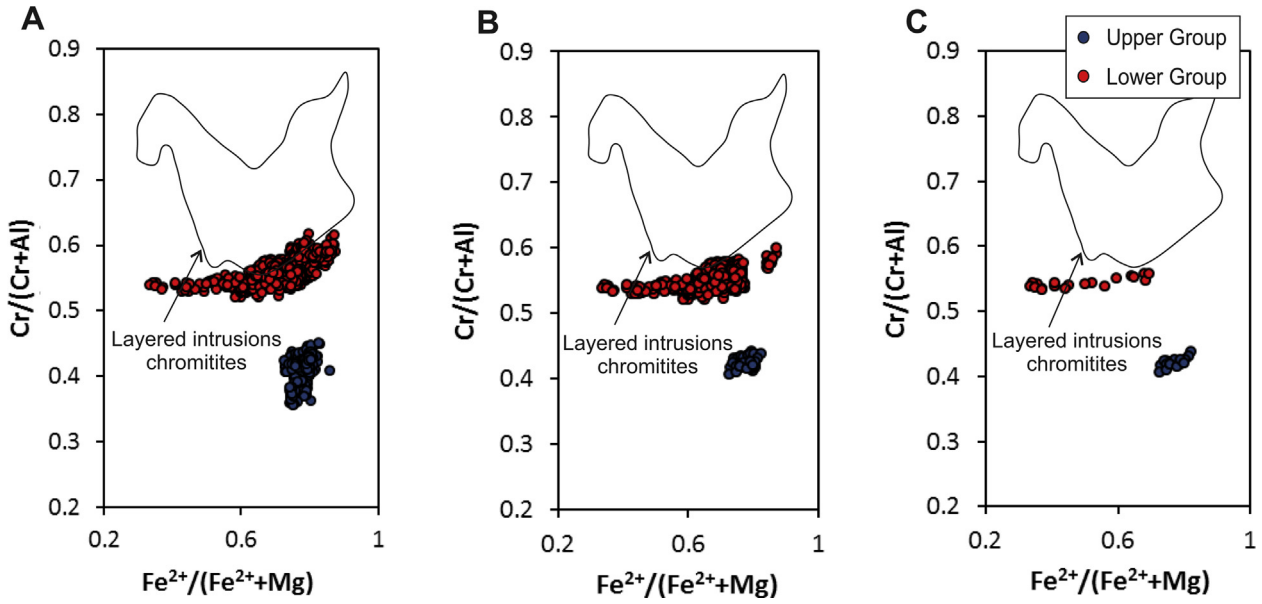

Fig. 12. $Fe^{2+}/(Mg + Fe^{2+})$ versus $Cr/(Cr + Al)$ of chromites from chromitites of the Luanga Complex. (A) Chromite analyses from all chromitites investigated. (B) Analyses of chromite from one chromitite of the Transition Zone (Lower Group) and one of the Mafic Zone (Upper Group). (C) Analyses of chromite from a traverse section of one representative chromite crystal from the chromitites indicated in (B). The field of chromite compositions in layered intrusions is from Barnes and Roeder (2001).

under greenschist and amphibolite facies have already been documented (Barnes, 2000; Mukherjee et al., 2010). Such processes could explain the entrapment of silicate minerals during chromite sintering. However, the observed features such as coalescence of inclusions, their rounded shape and even the sulfide accumulation at the bottom of inclusions do not favor this model. They suggest that these inclusions were formed during magmatic stage (i.e., melt inclusions). Therefore, we suggest that these inclusions were formed due to the entrapment of melt during chromite growth, a process that requires fast growth rate as described for chromite grains in komatiites (e.g., Arndt et al., 1977; Barnes, 1985; Godel et al., 2013) and modern picritic basalts (Roeder et al., 2001). High growth rate allows the crystallization of chromite with skeletal shapes and the entrapment of melt between dendritic branches (Fig. 14; Arndt et al., 1977). Different types of inclusion-bearing crystals, as described for chromitites from different stratigraphic portions of the Luanga Complex, would thus require different growth rates during the evolution of the complex. Chromite crystals hosting just one large inclusion demand lower growth rates than those hosting several inclusions, thus allowing the coalescence between the entrapped liquid and the development of just one inclusion (Fig. 14A). On the other hand, chromite crystals hosting several inclusions are formed under higher growth rates, allowing the entrapment of many physically isolated melt droplets in each crystal (Fig. 14B). High growth rate in chromite is generally related to high diffusion and cooling rates (Arndt et al., 1977; Barnes and Hill, 1995; Godel et al., 2013). This reasoning suggests that the entrapment of many silicate melt droplets within UGC is a response to higher cooling rates, caused by new primitive magma injections within mafic cumulates. In contrast, chromite crystals from LGC would have a slower growth rate due to no major difference in temperature between primitive magmas and hosting ultramafic cumulates.

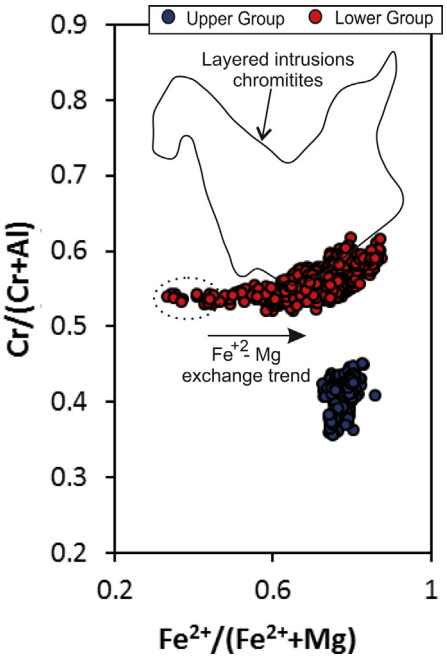

Fig. 13. $Fe^{2+}/(Mg + Fe^{2+})$ versus $Cr/(Cr + Al)$ of chromites from chromitites of the Luanga Complex. The dashed field indicates the composition of chromite from the main chromitite that likely represent compositions close to primary cumulus chromite of the Transition Zone. The field of chromite compositions in layered intrusions is from Barnes and Roeder (2001).

8. Conclusions

The principal conclusions of this study are as follows:

a. Chromitites in the Luanga Complex occur mainly in the upper portions of the Transition Zone, where they are hosted by ultramafic cumulates, and through the immediate contact with the overlying Mafic Zone, where they are hosted by plagioclase-bearing cumulates. This stratigraphic interval consists of several cyclic units interpreted as the result of successive influxes of primitive magma.
b. Chromite crystals in chromitites from the Transition Zone (i.e., Lower Group Chromitites - LGC) have distinctively higher Cr# compared with chromite crystals in chromitites

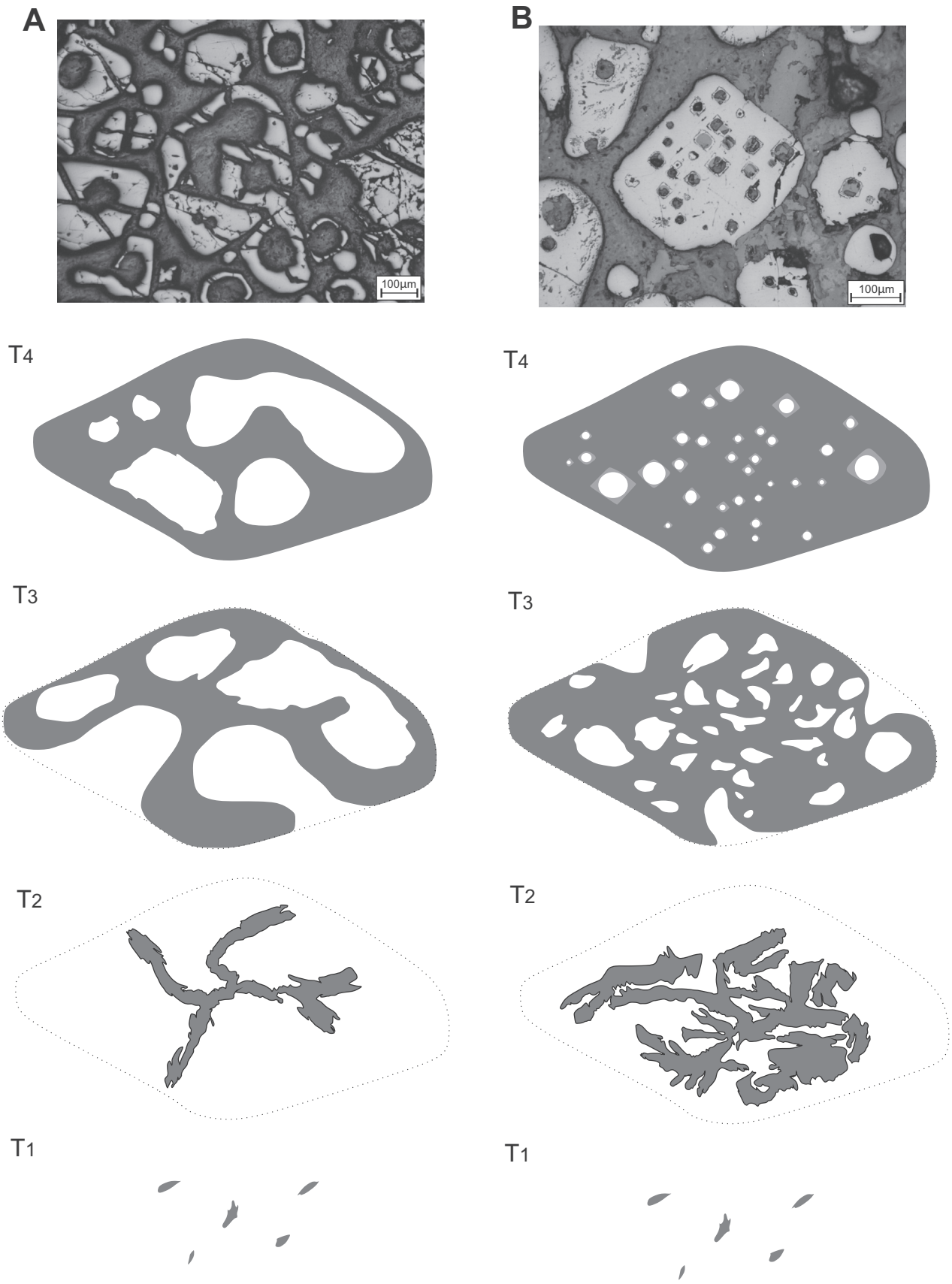

Fig. 14. Schematic model and photomicrographs illustrating the crystallization of different inclusion-bearing chromite grains. T1, T2, T3 and T4 represent the progressive evolution of the crystallization. (A) Crystallization of inclusion-bearing chromite crystals from chromitite of the Transition Zone (Lower Group). (B) Crystallization of inclusion-bearing chromite crystals from chromitite of the Mafic Zone (Upper Group).

from the Mafic Zone (i.e., Upper Group Chromitites - UGC). The upward decrease of Cr# in chromitites of the Luanga Complex matches the fractionation of the magma from ultramafic cumulates (olivine and/or orthopyroxene cumulates) in the Transition Zone to plagioclase-bearing cumulates in the Mafic Zone.

c. Extensive modification of primary cumulus composition of chromite in chromitite of the Luanga Complex is indicated by rimmed and/or extensively zoned chromite crystal. Zoned chromite indicates an extensive exchange between divalent (Mg, Fe^{2+}) cations and minor to none exchange between trivalent cations (Cr, Al and Fe^{3+}), and should result of subsolidus exchange of Fe^{2+} and Mg between chromite and coexisting silicates during slow cooling of the intrusion.

d. Significant modification of primary cumulus composition of chromite, as indicated in our study for the Luanga Complex, is likely to be common in non-massive chromitites and the rule for disseminated chromites in mafic intrusions. Therefore, the common use of spinel compositions as a petrogenetic indicator for mafic intrusions should be considered with caution.

Acknowledgements

This study was supported by CNPq (Conselho Nacional de Desenvolvimento Científico e Teconológico) and VALE S.A. (Projeto 550398/2010-4). Analytical facilities of the Instituto de Geociências of the University of Brasília (UNB) provided additional support for this research. The authors acknowledge VALE's Exploration Managers for Brazil and Carajás (Mr. Fernando Greco and Mr. Fernando Matos, respectively) for field support and access to exploration data. Cesar F. Ferreira Filho is a Research Fellow of CNPq and acknowledges the continuous support through research grants and scholarships for the "Metalogenênese de Depósitos Associados ao Magmatismo Máfico-Ultramáfico" Research Group. The authors thank the reviewers (Dr. Iain McDonald, and one anonymous) and guest editors (Dr. Sisir Mondal and Dr. Ria Mukherjee) for their constructive and helpful reviews. Federico Cuadros is thanked for assistance with electron microprobe analysis at the Universidade de Brasília. Eduardo T. Mansur holds a scholarship from Coordenação de Aperfeiçoamento de Pessoal de Nível Superior (CAPES – Brazil) and this study is part of his M.Sc. thesis developed at the Instituto de Geociências (Universidade de Brasília).

Appendix A. Supplementary data

Supplementary data associated with this article can be found, in the online version, at http://dx.doi.org/10.1016/j.oregeorev.2017.03.016.

References

Araújo, O.J.B., Maia, R.G.N., João, X.S.J., Costa, J.B.S., 1988. A megaestruturação arqueana da Folha Serra dos Carajás. Congresso Latino Americano de Geologia, Belém-Brazil, Anais, pp. 324-338.

Arndt, N.T., Naldrett, A.J., Pyke, D.R., 1977. Komatiitic and iron-rich tholeiitic lavas of Munro township, Northeast Ontario. J. Petrol. 18, 319–369.

Augé, T., 1987. Chromite deposits in the northern Oman ophiolite: Mineralogical constraints. Mineral. Deposita 22, 1–10.

Ballhaus, C.G., Stumpfl, E.F., 1986. Sulfide and platinum mineralization in the Merensky reef: evidence from hydrous silicates and fluid inclusions. Contrib. Mineral. Petrol. 94, 193–204.

Barnes, S.J., 1985. The petrography and geochemistry of Komatiite flows from the Abitibi greenstone-belt and a model for their formation. Lithos 18, 241–270.

Barnes, S.J., 1998. Chromite in komatiites, 1. Magmatic controls on crystallization and composition. J. Petrol. 39, 1689–1720.

Barnes, S.J., 2000. Chromite in komatiites, II modification during greenschist to mid – amphibolite facies metamorphism. J. Petrol. 41, 387–409.

Barnes, S.J., Hill, R.E.T., 1995. Poikilitic chromite in komatiitic cumulates. Mineral. Petrol. 54, 85–92.

Barnes, S.J., Roeder, P.L., 2001. The range of spinel compositions in terrestrial mafic and ultramafic rocks. J. Petrol. 42, 2279–2302.

Borisova, A., Ceuleneer, G., Kamenetsky, V., Arai, S., Bejina, F., Abily, B., Bindeman, I., Polve, M., de Parseval, P., Aigouy, T., Pokrovski, G.S., 2012. A new view on the petrogenesis of the Oman ophiolite chromitites from microanalyses of chromite-hosted inclusions. J. Petrol. 53, 2411–2440.

Danyushevsky, L.V., Della-Pasqua, F.N., Sokolov, S., 2000. Reequilibration of melt inclusions trapped by magnesian olivine phenocrysts from subduction-related magmas: Petrological implications. Contrib. Mineral. Petrol. 138, 68–83.

Dardenne, M.A., Ferreira Filho, C.F., Meirelles, M.R., 1988. The role of shoshonitic and calc-alkaline suites in the tectonic evolution of the Carajás District, Brazil. J. South Am. Earth Sci. 1, 363–372.

Diella, V., Ferrario, A., Girardi, V.A.V., 1995. PGE and PGM in the Luanga mafic-ultramafic intrusion in Serra dos Carajás (Pará State, Brazil). Ore Geol. Rev. 9, 445–453.

Docegeo - Rio Doce Geologia e Mineração, 1988. Revisão Litoestratigráfica da Província Mineral de Carajás. 35° Congresso Brasileiro de Geologia, Belém, Brasil, Anais, Sociedade Brasileira de Geologia, pp. 11–59.

Eales, H.V., Marsh, J.S., 1983. Al/Cr ratios of coexisting pyroxenes and spinelloids in some ultramafic rocks. Chem. Geol. 38, 57–74.

Eales, H.V., Reynolds, I.M., 1986. Cryptic variations within chromitites of the Upper Critical Zone, northwestern Bushveld Complex. Econ. Geol. 81, 1056–1066.

Evans, B.W., Frost, B.R., 1975. Chrome-spinel in progressive metamorphism - a preliminary analysis. Geochim. Cosmochim. Acta 39, 959–972.

Feio, G.R.L., Dall'Agnol, R., Dantas, E.L., Macambira, M.J.B., Santos, J.O.S., Althoff, F.J., Soares, J.E.B., 2013. Archean granitoid magmatism in the Canaã dos Carajás area: Implications for crustal evolution of the Carajás province, Amazonian craton, Brazil. Precambrian Res. 227, 157–185.

Ferreira Filho, C.F., Cançado, F., Correa, C., Macambira, E.M.B., Siepierski, L., Brod, T.C. J., 2007. Mineralizações estratiformes de EGP-Ni associadas a complexos acamadados em Carajás: os exemplos de Luanga e Serra da Onça. In: Publitec Gráfica & Editora, Contribuições à Geologia da Amazônia, vol. 5, pp. 01–14.

Gibbs, A.K., Wirth, K.R., Hirata, W.K., Olszewski Jr, W.J., 1986. Age and composition of the Grão Pará Group volcanics, Serra dos Carajás. Rev. Bras. Geoc. 16, 201–211.

Godel, B.M., Barnes, S.J., Gurer, D., Austin, P., Fiorentini, M.L., 2013. Chromite in komatiites: 3D morphologies with implications for crystallization mechanisms. Contrib. Mineral. Petrol. 165, 173–189.

Gole, M.J., Hill, R.E.T,. 1990. The refinement of extrusive models for the genesis of nickel deposits: implications from case studies at Honeymoon well and the walter Williams formations. Minerals and Energy Res. Institute of Western Australia Report. 68-93.

Haggerty, S.E., 1976. Opaque mineral oxides in terrestrial igneous rocks, in: Oxide minerals 3, D. Rumble, ed., pp. 101–300, Mineral. Soc. Am.

Henderson, P., 1975. Reaction trends shown by chrome-spinels of the Rhum layered intrusion. Geochim. Cosmochim. Acta 39, 1035–1044.

Henderson, P., Wood, R.J., 1981. Reaction relationships of chrome spinels in igneous rocks.Further evidence from the layered intrusions of Rhum and Mull, Inner Hebrides, Scotland. Contrib. Mineral Petrol. 78, 225–229.

Holdsworth, R.E., Pinheiro, R.V.L., 2000. The anatomy of shallow-crustal transpressional structures: insights from the Archean Carajás fault zone, Amazon, Brazil. J. Structural Geol. 61, 1105–1123.

Hulbert, L.J., Von Gruenewaldt, G., 1985. Textural and compositional features of chromite in the lower and critical zones of the bushveld complex South of Potgietersrus. Econ. Geol. 80, 872–895.

Irvine, T.N., 1965. Chromian spinel as a petrogenetic indicator. Part 1. Theory. Can. J. Earth Sci. 2, 648–672.

Irvine, T.N., 1977. Origin of chromite layers in the Muskox intrusion and other stratiform intrusions: a new interpretation. Geology 5, 273–277.

Li, C., Ripley, E.M., Sarkar, A., Shin, D., Maier, W.D., 2005. Origin of phlogopite-orthopyroxene inclusions in chromites from the Merensky Reef of the Bushveld Complex, South Africa. Contrib. Mineral. Petrol. 150, 119–130.

Liipo, J.P., Vuollo, J.I., Nykanen, V.M., Piirainen, T.A., 1995. Zoned Zn-rich chromite from the Naataniemi serpentinite massif, Kuhmo greenstone belt, Finland. Can. Mineral. 33, 537–545.

Lorand, J.P., Ceuleneer, G., 1989. Silicate and base-metal sulfide inclusions in chromites from de Maqsad area (Oman ophiolite): a model for entrapment. Lithos 22, 173–190.

Lorand, J.P., Cottin, J.Y., 1987. Na-Ti-Zr-H_2O-rich mineral inclusions indicating postcumulus chrome-spinel dissolution and recrystallization in the Western laouni mafic intrusion, Algeria. Contrib. Mineral. Petrol. 97, 251–263.

Macambira, M.J.B., Lancelot, J.R., 1996. Time Constraints for the Formation of the Archean Rio Maria Crust, Southeastern Amazonian Craton, Brazil. Int. Geol. Rev. 38, 1134–1142.

Machado, W., Lindenmayer, Z.G., Krogh, T.E., Lindenmayer, D., 1991. U-Pb geochronology of Archean magmatism and basement reactivation in the Carajás area, Amazon shield, Brazil. Precambrian Res. 49, 329–354.

Maier, W.D., Barnes, S.-J., 2008. Platinum-group elements in the UG1 and UG2 chromitites, and the Bastard Reef, at Impala platinum mine, Western Bushveld Complex, South Africa: evidence for late magmatic cumulate instability and reef constitution. S. Afr. J. Geol. 111, 159–176.

Mansur, E.T., Ferreira Filho, C.F., 2016. Magmatic structure and geochemistry of the Luanga Mafic-Ultramafic Complex: further constraints for the PGE-mineralized magmatism in Carajás, Brazil. Lithos 266–267, 28–43.

Marques, J.C., Ferreira Filho, C.F., 2003. The chromite deposits of the Ipueira-Medrado Sill, Bahia, Brazil. Econ. Geol. 98, 87–108.
Mondal, S.K., Mathez, E.A., 2007. Origin of the UG2 chromitite layer, Bushveld Complex. J. Petrol. 48, 495–510.
Mondal, S.K., Ripley, E.M., Li, C., Frei, R., 2006. The genesis of Archaean chromitites from the Nuasahi and Sukinda massifs in the Singhbhum craton, India. Precambrian Res. 148, 45–66.
Mukherjee, R., Mondal, S.K., González-Jimenez, J.M., Griffin, W.L., Pearson, N.J., O'Reilly, S.Y., 2015. Trace-element fingerprints of chromite, magnetite and sulfides from the 3.1 Ga ultramafic-mafic rocks of the Nuggihalli greenstone belt, Western Dharwar craton (India). Contrib. Mineral. Petrol. 169, 1–23.
Mukherjee, R., Mondal, S.K., Rosing, M.T., Frei, R., 2010. Compositional variations in the Mesoarchean chromites of the Nuggihalli schist belt, Western Dharwar craton (India): potential parental melts and implications for tectonic setting. Contrib. Mineral. Petrol. 160, 865–885.
Naldrett, A.J., Kinnaird, J., Wilson, A., Yudovskaya, M., McQuade, S., Chunnett, G., Stanley, C., 2009. Chromite composition and PGE content of Bushveld chromitites: part 1: the lower and middle groups. Appl. Earth Sci. IMM Trans. B. 118 (3), 131–161.
Naldrett, A.J., Wilson, A., Kinnaird, J., Yudovskaya, M., Chunnett, G., 2012. The origin of chromitites and related PGE mineralization in the Bushveld Complex: new mineralogical and petrological constraints. Mineral. Deposita 47, 209–232.
O'Driscoll, B., Emeleus, C.H., Donaldson, C.H., Daly, J.S., 2010. Cr-spinel seam petrogenesis in the Rhum layered suite, NW Scotland: cumulate assimilation and in situ crystallization in a deforming crystal mush. J. Petrol. 51, 1171–1201.
Pidgeon, R.T., Macambira, M.J.B., Lafon, J.M., 2000. Th-U-Pb isotopic systems and internal structures of complex zircons from an enderbite from the Pium Complex, Carajás Province, Brazil: evidence for the ages of granulite facies metamorphism and the protolith of the enderbite. Chem. Geol. 166, 159–171.
Power, M.R., Pirrie, D., Andersen, J.C.Ø., Wheeler, P.D., 2000. Testing the validity of chrome spinel chemistry as a provenance and petrogenetic indicator. Geology 28, 1027–1030.
Robin, E., Bonté, P., Froget, L., Jéhanno, C., Rocchia, R., 1992. Formation of spinels in cosmic objects during atmospheric entry: A clue to the Cretaceous-Tertiary boundary event. Earth Planet. Sci. Lett. 108, 181–190.
Roeder, P.L., Campbell, I.H., 1985. The effect of postcumulus reactions of composition of chrome-spinels from the Jimberlana Intrusion. J. Petrol. 26, 763–786.
Roeder, P.L., Poustovetov, A., Oskarsson, N., 2001. Growth forms and composition of chromian spinel in MORB magma: Diffusion-controlled crystallization of chromian spinel. Can. Mineral. 39, 397–416.
Rosa, W.D., 2014. Complexos acamadados da Serra da Onça e Serra do Puma: Geologia e petrologia de duas intrusões Máfico-Ultramáficas com sequência de cristalização distinta na Província Arqueana de Carajás, Brasil (Unpublished M. Sc. Thesis). Universidade de Brasília, Brazil, p. 65.
Sack, R.O., Ghiorso, M.S., 1991. An internally consistent model for the thermodynamic properties of Fe-Mg-titanomagnetite-aluminate spinels. Contrib. Mineral. Petrol. 106, 474–505.
Siepierski, L., Ferreira Filho, C.F., 2016. Spinifex-textured komatiites in the south border of the Carajas ridge, Selva Greenstone belt, Carajás Province, Brazil. J. South Am. Earth Sci. 66, 41–55.
Siepierski, L., 2016. Geologia, petrologia e potencial para mineralizações magmáticas dos corpos máfico-ultramáficos da região de Canaã dos Carajás, Província Mineral de Carajás, Brasil (Unpublished Ph.D. Thesis). Universidade de Brasília, Brazil, p. 156.
Souza, Z.S., Potrel, A., Lafon, J.M., Althoff, F.J., Pimentel, M.M., Dall'Agnol, R., Oliveira, C.G., 2001. Nd, Pb and Sr isotopes in the Identidade Belt, an Archean greenstone belt of Rio Maria region (Carajás Province, Brazil): implications for the geodynamic evolution of the Amazonian Craton. Precambrian Res. 109, 293–315.
Spandler, C., Mavrogenes, J., Arculus, R., 2005. Origin of chromitites in layered intrusions: Evidence from chromite-hosted melt inclusions from the Stillwater Complex. Geology 33, 893–896.
Spier, C.B., Ferreira Filho, C.F., 2001. The chromite deposits of the Bacuri mafic-ultramafic layered complex, Guyana shield, Amapá State, Brazil. Econ. Geol. 96, 817–835.
Stowe, C.W., 1994. Compositions and tectonic settings of chromite deposits through time. Econ. Geol. 89, 528–546.
Teixeira, J.B.G., Eggler, D.H., 1994. Petrology, Geochemistry, and Tectonic Setting of Archaean Basaltic and Dioritic Rocks from the N4 Iron Deposit, Serra dos Carajás, Pará, Brazil. Acta Geol. Leopoldensia 17, 71–114.
Teixeira, A.S., Ferreira Filho, C.F., Giustina, M.E.S.D., Araujo, S.M., Silva, H.H.A.B., 2015. Geology, petrology and geochronology of the Lago Grande layered complex: Evidence for a PGE-mineralized magmatic suite in the Carajás Mineral Province, Brazil. J. South Am. Earth Sci. 64, 116–138.
Vasquez, M.L., Carvalho, J.M.A., Sousa, C.S., Ricci, P.S.F., Macambira, E.M.B., Costa, L.T. R., 2008. Mapa Geológico do Pará em SIG. Brazilian Geological Survey - CPRM.
Villas, R.N., Santos, M.D., 2001. Gold deposits of the Carajás Mineral Province: deposit types and metallogenesis. Mineral. Deposita 36, 300–331.
Voordouw, R., Gutzmer, J., Beukes, N.J., 2009. Intrusive origin for Upper Group (UG1, UG2) stratiform chromitite seams in the Dwars River area, Bushveld Complex, South Africa. Mineral. Petrol. 97, 75–94.